A LOCATION-DEPENDENT SIGNAL-TO-INTERFERENCE RATIO ANALYSIS IN CELLULAR NETWORKS

A Thesis

Submitted to the Graduate School
of the University of Notre Dame
in Partial Fulfillment of the Requirements
for the Degree of

Master of Science
in
Electrical Engineering

by

Ke Feng

Martin Haenggi, Director

Graduate Program in Electrical Engineering
Notre Dame, Indiana

April 2019

CONTENTS

FIGURES

SYMBOLS

Φ	base station point process
λ	intensity of Φ
$\lvert\cdot\rvert$	Lebesgue measure
$\mathbb{P}$	probability measure
$\mathbb{E}$	expectation
$\mathbb{R}^d$	d-dimensional Euclidean space
$\lVert x\rVert$	Euclidean metric of $x \in \mathbb{R}^d$
o	origin of $\mathbb{R}^d$
$x_i(o)$	the i-th nearest BS to o
γ	cooperation level
$\mathcal{C}_i$	the i-th region
G	asymptotic SIR gain
$\mathcal{S}$	set of cooperating BSs
N	size of the cooperation set
α	path loss exponent
$\mathbb{1}(\cdot)$	indicator function
K	number of tiers
Φ_i	i-th tier base station point process
λ_i	intensity of Φ_i
P_i	power of Φ_i

ACKNOWLEDGMENTS

I would like to thank my advisor, Dr. Martin Haenggi, who always listens with patience, asks with insights and answers with preciseness. I benefited as much from his acts as from his words. Without his guidance this work would not have been possible.

I would like to thank Dr. Bertrand Hochwald and Dr. J. Nicholas Laneman. It is a privilege to have them as my committee members. I benefited a great deal from Dr. Hochwald's classes.

I would like to thank my colleagues Shuai, Jeya, Sanket, Abbas, Arash, Kang and folks at 250 for the technical and casual discussions we have on a daily basis. I benefited a lot from them.

The support from the U.S. NSF (grant CCF 1525904) is gratefully acknowledged.

Finally, I would like to thank my family and my friends for their love and support.

CHAPTER 1

INTRODUCTION

1.1 Background

The past three decades have witnessed a boost of data exchange and number/diversity of connected devices in the wireless networks. The demand for data transmission over the wireless medium will continue to grow. A key enabling factor to meet this demand is the densification and heterogeneity of base station (BS) deployment, along with other dimensions such as a new spectrum (millimeter band), more antennas (massive multiple-input and multiple-output technology), and coordinated transmissions. As the point-to-point transmission architecture is approaching its theoretical limit, integrating more BSs with diverse capabilities to the existing infrastructure provides the network with more available radio resources per unit area. Meanwhile, the coordination among massive active nodes brings potential gain, which is an essential part of advanced network design.

However, the analysis and design of current and future wireless systems are more challenging with the densification and heterogeneity of BS deployment. Modern communication scenarios rely on various performance aspects of the system including coverage, throughput, reliability, mobility, latency and so on. Having a guaranteed performance on each aspect is particularly important for cellular networks. Yet, the simulation of such a system is costly to implement, difficult if not impossible to replicate and insufficient for design insights. A specific simulation scenario often assumes numerous parameters, a deterministic network geometry and fixed transmission techniques. It leads to limited insights as to whether the network performance depends

on certain parameters, how it depends on them and why. Hence, the theoretical counterpart of simulations is needed, which (1) reflects the essential network characteristics, (2) permits the analysis of the network from various aspects, and (3) serves as a baseline to compare the performance of advanced transmission techniques.

Due to the nature of the wireless medium, any node in the network can in theory transmit/receive signals to/from other nodes. An inherent problem with such a freedom is interference. Interference has become the limiting factor in today's dense cellular networks. Since wireless signals are subject to multi-path fading and path loss, both desired signal and interference depend strongly on the geometric locations of the transmitting nodes. Network geometry, therefore, plays a critical role in the modelling of current networks.

By modelling the node locations in space as a random point process, stochastic geometry provides a natural tool for network analysis. The randomness of node locations is justified since real BS deployment is subject to constrains from various sources, and there is less planning of deployment with smaller and lower-cost BSs. In particular, modeling BS locations using the homogeneous Poisson point process (PPP) has become a common practice due to the tractability of the model. Prior to that, networks models were based on either a limited number of cells or the hexagonal lattice structure—one failed to capture the growing scale of the network and the other failed to capture the inherent randomness and heterogeneity [1]. Indeed, real BS deployment often falls in between ideal hexagonal lattice and the PPP [2]. The PPP model can (1) provide a theoretical lower bound of the network performance, and (2) facilitate the analysis of general networks models and advanced transmission techniques by approximation [3, 4].

Similar to the role of the signal-to-noise ratio (SNR) in point-to-point systems [5], the signal-to-interference ratio (SIR) is a critical quantity in dense networks. The SIR varies significantly with the distances from a user to both its transmitter(s)

and interferers. For instance, it is commonly acknowledged that "the cell boundary users" are the bottleneck of cellular networks due to their vulnerability to interference [6]. For practical system design such as interference management, handover and fairness mechanisms, characterizing the performance of "the cell boundary users" is important. However, the existing literature based on stochastic geometry focuses mostly on the typical user, who represents the average of all users. Hence, the goal of this thesis is to classify users by their vulnerability to interference and design advanced techniques to ameliorate the problem.

Interference can be mitigated through the coordination among transmissions. Coordination can be in the form of multi-user scheduling, relaying, joint transmission and so on. The gain comes at the cost of the channel state information (CSI), backhaul capacity, synchronization efforts, and in general more signaling overhead. Coordinated multipoint (CoMP) [7] is an effective technique to mitigate inter-cell interference and has been incorporated into the long-term evolution (LTE). By allowing selected BSs to jointly serve one or more users, the interference originating from nearby BSs can be turned into useful signals. In this thesis, we study a BS cooperation scheme that primarily helps users vulnerable to interference due to their disadvantaged locations. In order to put minimal constraints on the system, we focus on the analysis of non-coherent joint transmission.

1.2 Related Work

The general theory of stochastic geometry can be found in [8–10] and its application in wireless networks in [11–14]. We refer readers to [15–17] for an overview of the field. Stochastic geometry is extensively applied to the analysis of cellular networks from network modelling [2, 18–21], SIR/SINR characterization [3, 22–26], interference management and coordinated transmissions [25, 27–34], heterogeneous networks and load balancing [34–37], drone communications [38, 39] and so on. We

now give a more detailed literature review on BS cooperation.

BS cooperation schemes mainly focuses on four aspects: the dependence of cooperation on users' channel (user-centric or not), the selection of the set of cooperating BSs (fixed-size or adaptive), the cooperation mode (BS silencing, point selection, coherent/non-coherent joint transmission), and its implementation challenges (limited backhaul, imperfect synchronization, imperfect CSI). [30, 31, 33] study user-centric BS cooperation while [25, 34] study BS cooperation where all users are non-coherently served by n strongest BSs. It is shown in [34] that users located at the Voronoi vertices benefit more from cooperation than the typical user. Also, it is shown in [25] that increasing the size of the cooperation set leads to a larger variance of the link success probability and thus reduces fairness. In [31, 33], the authors define the "cooperation region" such that users receive cooperation only when they are located in the cooperation region. Both definitions are based on the relative distances to the serving and the nearest interfering BS, and different cooperation modes are analyzed. In [33], BS silencing is activated for users in the cooperation region. However, it assumes a small-cell scenario where there are many inactive BSs and is thus less interference-limited. [31] studies the network where all BSs are always active. Users within the cooperation region are coherently served by the two nearest BSs. The scheme, however, relies on the precise channel phase match within the cooperating BSs. A transmission scheme that is less sensitive to channel estimation is analyzed in [30], where the cooperating BSs non-coherently transmit to the target user without exchanging CSI. The set of cooperating BSs is defined to be BSs within a disk of a fixed radius centered at each user. The definition depends on the selection of the radius and leads to an indefinite size of the cooperating set, which can boost the system complexity. BS cooperation in a two-tier network is studied in [36], where the strongest BSs from each tier jointly serve users who suffer from strong interference. The scheme does not consider the case when both the strongest serving BS and

strongest interfering BS belong to the same tier.

1.3 Contributions

This thesis makes the following main contributions:

1. We mathematically define the cell regions for any ergodic and stationary BS point process based on the relative distances of the three nearest BSs. While we focus on Rayleigh fading and power-law path loss, the user grouping method is based on the relative average received signal strengths of the three strongest BSs, which applies to general channel models and heterogeneous networks.

2. We show that in Poisson networks, the top fraction x of users enjoy an SIR gain of $-5\alpha \log_{10} x$ dB relative to the typical user. We derive both the exact and asymptotic form of the SIR distribution for the cell boundary users.

3. We propose and study a location-dependent BS cooperation scheme which primarily helps users vulnerable to interference. We introduce a parameter $\gamma \in [0, 1]$ to tune the cooperation level of the network. We derive the SIR distribution and its approximation form based on the asymptotic SIR gain.

4. We show that in Poisson networks (1) the derivative of the asymptotic SIR gain equals to the path loss exponent α at $\gamma = 0$ (no cooperation) and is 0 at $\gamma = 1$ (full cooperation); (2) a moderate γ jointly improves the SIR performance and the network fairness.

5. We study the spectral efficiency normalized by the number of cooperating BSs. The normalization permits the evaluation of BS cooperation gain without increasing the cell load, *i.e.*, users who receive cooperation from N BSs are served by $1/N$ resource blocks from each BS. We show that with a moderate γ, the non-coherent joint transmission can improve users' throughput even with the normalization.

6. In each case, network models including the PPP, lattice networks and heterogeneous networks (used interchangeably with "multi-tier networks") are studied. We compare the simulation results of the asymptotic SIR gain in lattice networks to Poisson networks and show their similarity. Multi-tier networks consider different powers and densities of each tier of BSs.

1.4 Thesis Organization

In Chapter 2, we describe the system model and introduce performance metrics to characterize the SIR. Specifically, BS models including the PPP, lattice networks,

and heterogeneous networks (used interchangably with "multi-tier networks" in this thesis) are introduced. Metrics including the success probability (known also as the coverage probability or the complement of the outage probability in the literature), the asymptotic SIR gain, the conditional success probability, and the SIR meta distribution are introduced.

In Chapter 3, we introduce the definition of the cell center region and the cell boundary region for any ergodic and stationary point process. We analyze the SIR performance based on a user's located region.

In Chapter 4, we design a location-dependent BS cooperation scheme based on the definition from Chapter 3. The cell partition is extended to three regions: the cell center region, the cell edge region and the cell corner region. The rationale behind this partition is that the worst-case user located on the vertex of Voronoi cells has three equidistant nearest BSs.

We include conclusions and future work in Chapter 5.

CHAPTER 2

SYSTEM MODEL AND CHARACTERIZATIONS OF THE SIR

In this chapter, we introduce the system model and performance metrics. In the first section, we introduce three BS models: the homogeneous PPP (also referred to as "Poisson networks"), stationary lattices, and heterogeneous networks. In general, the actual deployment of BSs falls somewhere between Poisson networks and lattice networks—from completely random to completely repulsive [2]. The study of the homogeneous PPP model potentially provides unified analysis that applies to general network models. For the channel model, we consider iid Rayleigh fading and power-law path loss.

In the second section, we introduce metrics that characterize the SIR performance, from the most coarse characterization—the success probability of the typical user, to the most fine-grained one—the SIR meta distribution. The most extensively explored metric is the success probability, which is the probability that the SIR exceeds a threshold θ. For less tractable models, we use the PPP model as a baseline to approximate the success probability [22]. Specifically, the asymptotic SIR gain captures the SIR gap between different models as $\theta \to 0$ and is shown to be a good approximation over the entire range of θ. Further, the conditional success probability and its distribution the SIR meta distribution are introduced to answer questions like "*what is the fraction of links in the network that achieve an SIR of 5 dB with 90% of the time?*".

2.1 System Model

We first give the definition of a Voronoi cell for general point process. Then we define three BS models, namely the homogeneous PPP, stationary lattices and heterogeneous networks.

Definition 1. *The Voronoi cell $V(x)$ of a point x of a general point process $\Phi \subset \mathbb{R}^d$ consists of those locations of $\mathbb{R}^d$ whose distance to x is not greater than their distance to any other point in Φ, i.e.,*

$$V(x) \triangleq \{u \in \mathbb{R}^d \colon \|x-u\| \leq \|z-u\| \ \forall z \in \Phi \setminus \{x\}.\} \tag{2.1}$$

2.1.1 Homogeneous PPP

Definition 2. *The homogeneous PPP with intensity λ is a point process in $\mathbb{R}^d$ such that*

- *for every compact set B, the number of points falling into B has a Poisson distribution with mean $\lambda|B|$, where $|B|$ is the Lebesgue measure of B.*
- *the numbers of points in disjoint bounded sets are independent random variables.*

The intensity λ is the expected number of points of the process per unit area or volume.

2.1.2 Stationary Lattices

Definition 3. *Let $\mathbb{L} \subset \mathbb{R}^d$ be a lattice and $V(o)$ the Voronoi cell of the origin. The randomly translated lattice is*

$$\Phi \triangleq \{u \in \mathbb{Z}^d \colon \mathbf{G}u + X\} \tag{2.2}$$

where $\mathbf{G} \in \mathbb{R}^{d \times d}$ is an arbitrary matrix of full rank and X is uniformly distributed over $V(o)$.

In the case of (stationary) triangular lattice, $\mathbf{G} = \eta \begin{bmatrix} 1 & 1/2 \\ 0 & \sqrt{3}/2 \end{bmatrix}$ and the density of Φ is $2/(\sqrt{3}\eta^2)$.

2.1.3 Multi-Tier Networks

We model heterogeneous networks by the union of K BS point process, *i.e.*,

$$\Phi \triangleq \bigcup_{i=1}^{K} \Phi_i \tag{2.3}$$

where Φ_i is a stationary and ergodic BS point process. We only specify two parameters for Φ_i: the density λ_i and the transmit power P_i. No assumption about the independence/dependence between Φ_is is made to preserve the generality of the model. Since the selection of proper model for each tier is a dedicated research problem itself, we only propose the definition of cell regions in heterogeneous networks and study a special case when the network tiers are modeled by independent PPPs.

We will focus on the power-law path loss model, *i.e.*,

$$l(r) = r^{-\alpha}, \tag{2.4}$$

where r denotes the distance from the transmitter to the receiver. $l(r)$ denotes the mean power received at distance r when unit power is transmitted, and $\alpha > 2$ is the path loss exponent. We assume iid Rayleigh fading from different BSs. Denote h as the power of the multiplicative fading, where

$$\mathbb{P}(h > x) = \exp(-x), \quad x \geq 0. \tag{2.5}$$

The SIR is defined as

$$\text{SIR} \triangleq \frac{S}{I}, \tag{2.6}$$

where S denotes the desired signal power and I denotes the aggregated power of interference. The most basic model is when the desired signal comes from one selected serving BS and the interference comes from the other transmitting BSs. In this thesis, we will use maximum-average-signal-strength association, *i.e.*, nearest-neighbor association, as the baseline model. We focus on the typical user[1] located at the origin. Let $x_i(o) \in \Phi$ denote the i-th nearest BS to the origin, h_i denote the fading from $x_i(o)$ and $r_i = \|x_i(o)\|$ denote the Euclidean distance from $x_i(o)$ to the origin,

$$\text{SIR} = \frac{h_1 r_1^{-\alpha}}{\sum_{i>1} h_i r_i^{-\alpha}}. \tag{2.7}$$

2.2 Characterizations of the SIR

2.2.1 Success Probability

For a given threshold θ, the success probability is defined as

$$\bar{F}(\theta) \triangleq \mathbb{P}(\text{SIR} > \theta), \tag{2.8}$$

which is the complementary cumulative distribution function (CCDF) of the SIR.

In this thesis, we will use $\bar{F}_{\text{PPP}}(\theta)$ to denote the success probability for the homogeneous PPP with intensity λ, it is shown in [18, 28]

$$\bar{F}_{\text{PPP}}(\theta) = \frac{1}{{}_2F_1(1, -\delta; 1-\delta; -\theta)}, \tag{2.9}$$

where $\delta = 2/\alpha$ and ${}_2F_1(,;;)$ is the Gaussian hypergeometric function.

[1]The performance of the typical user corresponds to the average performance of all users in the network. By the stationarity of the point process, we assume that the typical user is located at the origin without loss of generality.

2.2.2 Asymptotic SIR Gain

While the success probability of all but a few basic network models is intractable, the asymptotic SIR gain [22] gives a simple and unified characterization of the SIR improvement compared to a baseline scheme. Using the PPP model as baseline, G is the asymptotic SIR gain if

$$\bar{F}(\theta) \sim \bar{F}_{\text{PPP}}(\theta/G), \quad \theta \to 0. \tag{2.10}$$

It can be visualized as the asymptotic horizontal shift (in dB) between the SIR distributions of the studied model and the PPP.

Lemma 1. *For Rayleigh fading [22],*

$$\bar{F}(\theta) \sim \theta \mathbb{E}[I/\bar{S}], \quad \theta \to 0. \tag{2.11}$$

where $\bar{S} \triangleq \mathbb{E}_h(S)$.

Proof.

$$\begin{aligned} \bar{F}(\theta) &= \mathbb{P}(\text{SIR} > \theta) \\ &= \mathbb{P}(h > \theta I/\bar{S}) \\ &= \mathbb{E}[\exp(-\theta I/\bar{S})] \\ &\sim \theta \mathbb{E}[I/\bar{S}], \quad \theta \to 0. \end{aligned} \tag{2.12}$$

□

Following [22], we define the mean-interference-signal-ratio (MISR) as $\text{MISR} \triangleq \mathbb{E}\big(I/\bar{S}\big)$. MISR_{PPP} denotes the MISR of the PPP. Using Lemma 1 and the PPP

model as baseline, we have

$$\bar{F}(\theta) \sim \bar{F}_{\mathrm{PPP}}(\theta/G), \quad \theta \to 0, \tag{2.13}$$

where $G \triangleq \mathrm{MISR}_{\mathrm{PPP}}/\mathrm{MISR}$ is the asymptotic SIR gain.

It is shown that the asymptotic gain is an accurate approximation to capture the difference for the SIR distribution of different network models over the entire range of θ [3]. The form of $\bar{F}(\theta)$ depends on the fading statistics and generalizes to other fading models.

2.2.3 Conditional Success Probability

For an individual link with fixed locations of the user and BSs, the conditional success probability for a SIR threshold θ is defined as

$$P_{\mathrm{s}}(\theta) \triangleq \mathbb{P}(\mathrm{SIR} > \theta \mid \Phi), \tag{2.14}$$

where Φ denotes the set of active BSs. It is also referred to as the individual link reliability, quantifying how reliable the link is with respect to θ. The quantity $P_{\mathrm{s}}(\theta) \in [0, 1]$ is obtained by averaging over fading only.

For Rayleigh fading and power-law path loss,

$$P_{\mathrm{s}}(\theta) = \prod_{i=2}^{\infty} \frac{1}{1 + \theta r_1^{\alpha}/r_i^{\alpha}}. \tag{2.15}$$

The traditional success probability can be obtained by the expectation of the conditional link success probability over the point process, *i.e.*,

$$\bar{F}(\theta) = \mathbb{E}[P_{\mathrm{s}}(\theta)]. \tag{2.16}$$

2.2.4 SIR Meta Distribution

By defining the conditional success probability, the randomness in time (fading) and space (BS point process) can be separately evaluated, thus providing a finer-grained view of the SIR. The distribution of the conditional success probability can characterize the link performance in cellular networks. It answers questions such as "*what is the fraction of links in the network that achieve an SIR of 5 dB with 90% of the time?*". The SIR meta distribution (MD) [24], defined as

$$\bar{F}_{P_{\mathrm{s}}}(\theta, x) \triangleq \mathbb{P}(P_{\mathrm{s}}(\theta) > x), \quad x \in [0, 1], \tag{2.17}$$

is the fraction of links achieving reliability higher than x for threshold θ. For an ergodic BS point process, the SIR MD distribution can be interpreted as the fraction of links that achieves θ and reliability higher than x in any realization of the network.

Fig. 2.1 shows the histogram of the individual link reliability for $\theta = 1$ in a Poisson network via simulation. In this example, when the target reliability is set to be $x = 0.56$ (which is the success probability of the typical user), the empirical value of the fraction of links satisfying $P_{\mathrm{s}}(1) > 0.56$ is 0.5 and they are referred to as "top 50% users". The mean is coincidentally equal to the median for the parameters in this example.

Fig. 2.2 shows the color map of the individual link reliability in the Voronoi cells. It is obvious from observation and intuitive that users in the cell center region achieve better average performance than the typical user due to their good locations.

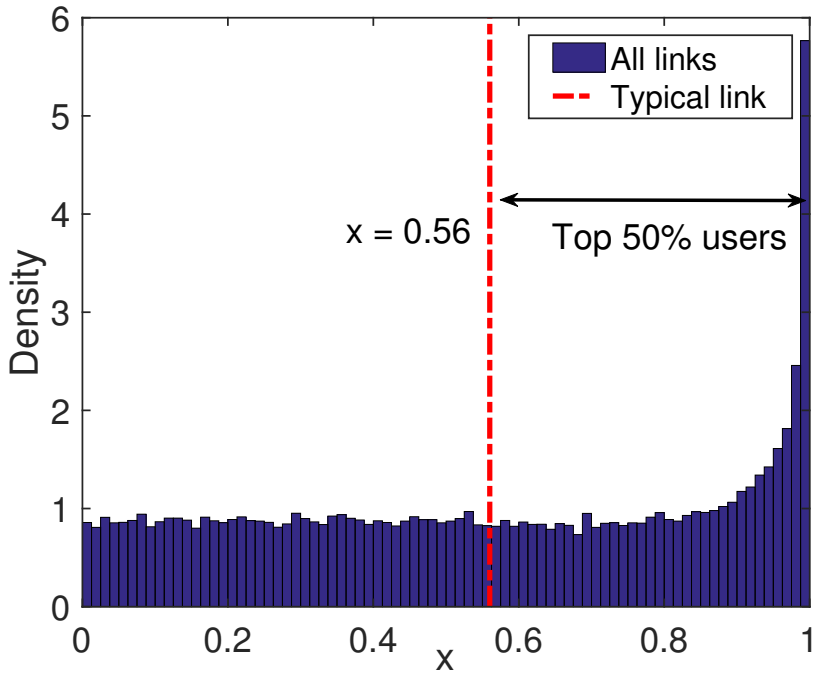

Figure 2.1. Histogram of the conditional success probability for a PPP network, $\alpha = 4$. $\mathbb{P}(P_{\mathrm{s}}(\theta) > 0.56) \approx 0.5$.

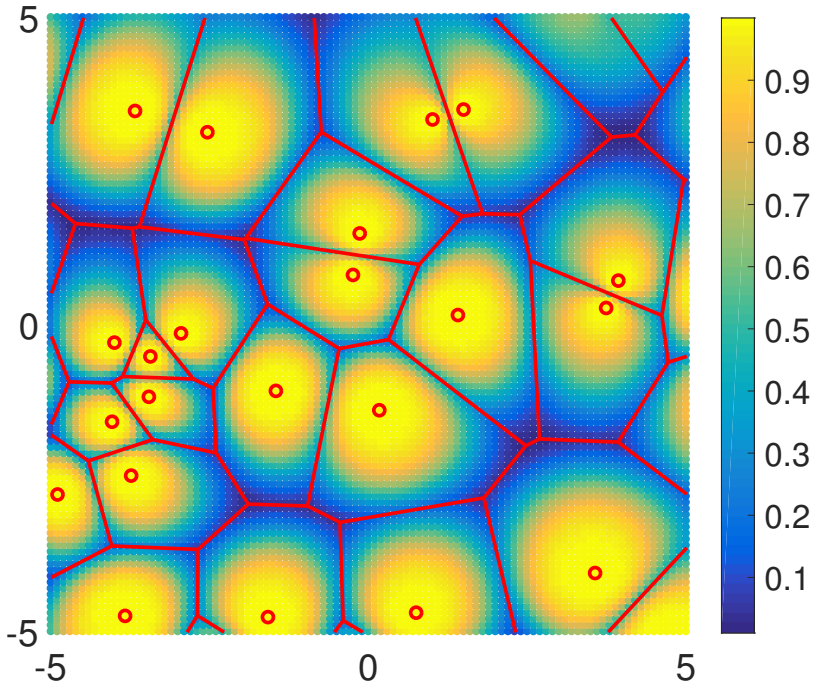

Figure 2.2. The color map of the conditional success probability for a realization of a PPP network with intensity $\lambda = 1$, $\alpha = 4$.

CHAPTER 3

LOCATION-DEPENDENT SIR ANALYSIS

In the literature, "the cell boundary users" typically refers to users who are almost equally close to the serving and nearest interfering BS, and "the cell center users" refers to those who are much closer to the serving BS than to interfering ones. It is equally common to define these merely by users' distance to the serving BS. The latter one is deficient since cells have random sizes. Users within the defined radius of the serving BS can be subject to strong interference and users outside the radius of the serving BS do not necessarily suffer from strong interference. In this chapter, we partition the Voronoi cells of any stationary and ergodic BS process into the cell center region and the cell boundary region based on the relative distance to two nearest BSs. The intuition is that the SIR is mostly affected by the ratio of the desired signal to the first-order interference. We study the SIR distribution of the typical user in each region. We show a surprisingly simple relationship between the SIR performance of the typical cell center user and that of the typical user in Poisson networks: the top fraction x of users enjoy an SIR gain of $-5\alpha \log_{10} x$ dB relative to the typical user for the power-law path loss with the exponent α. For the cell boundary users, both the exact form and approximation based on the asymptotic SIR gain are given[1].

The idea of grouping users and analyzing the corresponding performance applies to general networks. In the case of heterogeneous networks, the transmission power, BS density and load balancing can be integrated to the definition of cell regions.

[1]Part of this chapter has been presented at [40].

3.1 Cell Partition

We define the region of a location u by how much closer u is to its serving BS than to its nearest interfering BS following [29, 31]. Let $\Phi \subset \mathbb{R}^2$ be an ergodic and stationary BS point process and $x_i(u) \in \Phi$ be the i-th nearest BS to u. For $\gamma \in [0,1]$ and $\rho = 1-\gamma$

$$\begin{aligned} \mathcal{C}_1 &\triangleq \{u \in \mathbb{R}^2 \colon \|u - x_1(u)\| \leq \rho \|u - x_2(u)\|\} \\ \mathcal{C}_2 &\triangleq \{u \in \mathbb{R}^2 \colon \rho \|u - x_2(u)\| < \|u - x_1(u)\|\}. \end{aligned} \tag{3.1}$$

Here, $\mathcal{C}_1$ is referred to as the "cell center region" and $\mathcal{C}_2$ as the "cell boundary region". γ controls the area fraction of each region. $\gamma = 0$ is the case where $\mathcal{C}_1 = \mathbb{R}^2$ and $\gamma = 1$ is the case where $\mathcal{C}_2 = \mathbb{R}^2$

Using the geometric partition, we can express the success probability as

$$\bar{F}(\theta) = \sum_{i=1}^{2} \mathbb{P}(\mathrm{SIR} > \theta \mid o \in \mathcal{C}_i)\mathbb{P}(o \in \mathcal{C}_i). \tag{3.2}$$

In the next section, we will study the success probability conditioned on the typical user being in the two regions.

Let $r_i \triangleq \|x_i(o)\|$ denote the distance of the i-th nearest BS to o. For any stationary and ergodic BS point process, from (3.1),

$$\mathbb{P}(o \in \mathcal{C}_1) = \mathbb{P}\Big(\frac{r_1}{r_2} \leq \rho\Big), \quad \mathbb{P}(o \in \mathcal{C}_2) = \mathbb{P}\Big(\frac{r_1}{r_2} > \rho\Big). \tag{3.3}$$

3.2 Poisson Networks

Lemma 2. *For a homogeneous Poisson point process in $\mathbb{R}^m$ with intensity λ,*

$$\mathbb{P}\Big(\frac{r_i}{r_{i+1}} \leq x\Big) = x^{mi}, \quad x \in [0,1]. \tag{3.4}$$

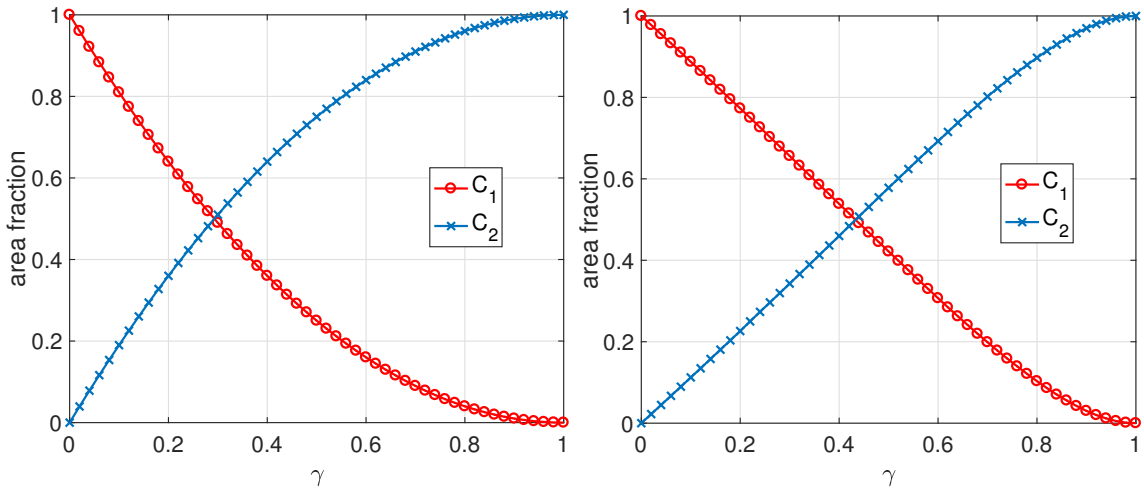

(a) Poisson networks. (b) Triangular lattice networks.

Figure 3.1. The area fraction of both regions.

Proof.

$$\begin{aligned}\mathbb{P}(r_i/r_{i+1} \le x) &= \mathbb{E}[\mathbb{P}(r_i/r_{i+1} \le x \mid r_{i+1})] \\ &= \mathbb{E}[\mathbb{P}(r_i \le x r_{i+1} \mid r_{i+1})] \\ &\overset{\text{(a)}}{=} x^{mi}.\end{aligned}$$

Step (a) follows from the fact that conditioning on r_{i+1}, the i points are independently and uniform randomly distributed in the m-dimensional ball with radius r_{i+1}. Thus, the distance ratio r_i/r_{i+1} is independent of the value of r_{i+1} for $i \in \mathbb{N}^+$. □

Lemma 2 gives the area fraction of both regions in Poisson networks, *i.e.*,

$$\mathbb{P}(o \in \mathcal{C}_1) = \rho^2, \quad \mathbb{P}(o \in \mathcal{C}_2) = 1 - \rho^2. \tag{3.5}$$

In the case when Φ is a lattice network, the calculation of the area fractions is straightforward but the result is unwieldy. Fig. 4.2 shows the area fraction of each region in Poisson networks and triangular networks as γ increases from 0 to 1.

Note that from Lemma 2, the random variable r_i/r_{i+1} is more likely to have a value close to 1 as i increases. It is intuitive since the void probability depends on the area of the annulus $\pi(r_i^2/x^2 - r_i^2)$, which depends on r_i.

Lemma 3. *For any PPP, the random variables* $r_1/r_2, r_2/r_3, ..., r_i/r_{i+1},\ i \in \mathbb{N}^+$ *are pairwise independent. i.e.,*

$$f_{\frac{r_i}{r_{i+1}},\frac{r_j}{r_{j+1}}}(x,y) = f_{\frac{r_i}{r_{i+1}}}(x) f_{\frac{r_j}{r_{j+1}}}(y), \quad \forall i \neq j,\ i,j \in \mathbb{N}^+. \tag{3.6}$$

Proof. It is sufficient to prove (3.6) for $j = i+1$ and $j > i+1$. For $j = i+1$,

$$\begin{aligned}
\mathbb{P}\Big(\frac{r_i}{r_{i+1}} \leq x, \frac{r_{i+1}}{r_{i+2}} \leq y\Big) &= \mathbb{E}\bigg[\mathbb{P}\Big(\frac{r_i}{r_{i+1}} \leq x, \frac{r_{i+1}}{r_{i+2}} \leq y \;\Big|\; r_{i+1}\Big)\bigg] \\
&\overset{(a)}{=} \mathbb{E}\bigg[\mathbb{P}\Big(\frac{r_i}{r_{i+1}} \leq x \;\Big|\; r_{i+1}\Big)\mathbb{P}\Big(\frac{r_{i+1}}{r_{i+2}} \leq y \;\Big|\; r_{i+1}\Big)\bigg] \\
&\overset{(b)}{=} \mathbb{P}\Big(\frac{r_i}{r_{i+1}} \leq x\Big)\mathbb{E}\bigg[\mathbb{P}\Big(\frac{r_{i+1}}{r_{i+2}} \leq y \;\Big|\; r_{i+1}\Big)\bigg] \\
&= \mathbb{P}\Big(\frac{r_i}{r_{i+1}} \leq x\Big)\mathbb{P}\Big(\frac{r_{i+1}}{r_{i+2}} \leq y\Big)
\end{aligned}$$

where (a) follows from the fact that for Poisson point processes, r_i is independent of r_{i+2} given r_{i+1}. (b) follows from the independence of r_i/r_{i+1} and r_{i+1} as established in the proof of Lemma 2.

For $i+1 < j$,

$$\begin{aligned}
\mathbb{P}\Big(\frac{r_i}{r_{i+1}} \leq x, \frac{r_j}{r_{j+1}} \leq y\Big) &= \mathbb{E}\bigg[\mathbb{P}\Big(\frac{r_i}{r_{i+1}} \leq x, \frac{r_j}{r_{j+1}} \leq y \;\Big|\; r_{i+1}, r_j\Big)\bigg] \\
&= \mathbb{E}\bigg[\mathbb{P}\Big(\frac{r_i}{r_{i+1}} \leq x \;\Big|\; r_{i+1}\Big)\mathbb{P}\Big(\frac{r_j}{r_{j+1}} \leq y \;\Big|\; r_j\Big)\bigg] \\
&= \mathbb{P}\Big(\frac{r_i}{r_{i+1}} \leq x\Big)\mathbb{E}\bigg[\mathbb{P}\Big(\frac{r_j}{r_{j+1}} \leq y \;\Big|\; r_j\Big)\bigg] \\
&= \mathbb{P}\Big(\frac{r_i}{r_{i+1}} \leq x\Big)\mathbb{P}\Big(\frac{r_j}{r_{j+1}} \leq y\Big).
\end{aligned}$$

□

Lemma 3 is a key result that helps simply the analysis related to relative distances in Poisson networks. Using the same technique, we can immediately show that r_1/r_2 is independent of r_2/r_i, for $\forall i \geq 2, i \in \mathbb{N}^+$.

3.2.1 Cell Center Region

Theorem 1. *For a homogeneous PPP, the success probability conditioned on the typical user lying in $\mathcal{C}_1$ is*

$$\mathbb{P}(\text{SIR} > \theta \mid o \in \mathcal{C}_1) = \bar{F}_{\text{PPP}}(\theta \rho^{\alpha}). \tag{3.7}$$

In particular, for $\alpha = 4$, we have

$$\mathbb{P}(\text{SIR} > \theta \mid o \in \mathcal{C}_1) = \frac{1}{1 + \rho^2 \sqrt{\theta} \arctan\left(\rho^2 \sqrt{\theta}\right)}. \tag{3.8}$$

Proof.

$$\begin{aligned}
\mathbb{P}(\text{SIR} > \theta \mid o \in \mathcal{C}_1) &= \mathbb{P}(S > \theta I \mid o \in \mathcal{C}_1) \\
&\overset{\text{(a)}}{=} \mathbb{E}\left[\prod_{i=2}^{\infty} \frac{1}{1 + \theta (\frac{r_1}{r_i})^{\alpha}} \mid o \in \mathcal{C}_1 \right] \\
&= \mathbb{E}\left[\prod_{i=2}^{\infty} \frac{1}{1 + \theta \rho^{\alpha} (\frac{r_1/\rho}{r_i})^{\alpha}} \mid o \in \mathcal{C}_1 \right] \\
&\overset{\text{(b)}}{=} \mathbb{E}\left[\prod_{i=2}^{\infty} \frac{1}{1 + \theta \rho^{\alpha} (\frac{r_1}{r_i})^{\alpha}} \right] \\
&= \bar{F}_{\text{PPP}}(\theta \rho^{\alpha}),
\end{aligned}$$

where step (a) follows from the fact that for Rayleigh fading, $\mathbb{P}(h > x) = \exp(-x)$ and the Laplace transform $\mathcal{L}_h(s) \triangleq \mathbb{E}[\exp(-sh)] = 1/(1+s)$. Step (b) is due to the fact that the region $\mathcal{C}_1$ is equivalent to $\{r_1/r_2 < \rho\} = \{r_1/\rho < r_2\}$. Put differently,

the probability law of $r_1/\rho, r_2, ...$ conditioned on $r_1/r_2 < \rho$ is the same as the law of $r_1, r_2, ...$ without conditioning. This can be shown by establishing that $f_{\frac{r_1}{\rho}}(x \mid \frac{r_1}{r_2} \leq \rho) = f_{r_1}(x)$ in the following derivation and using the independence from Lemma 3.

$$\begin{aligned}\mathbb{P}\left(r_1 \leq x \mid \frac{r_1}{r_2} < \rho\right) &= \frac{\mathbb{P}(r_1 \leq x, r_1/r_2 < \rho)}{\mathbb{P}\big(r_1/r_2 < \rho\big)} \\ &= \frac{\int_0^x \int_{\frac{u}{\rho}}^{\infty} 4\lambda\pi uv \exp\left(-\lambda\pi v^2\right) \mathrm{d}v \mathrm{d}u}{\rho^2} \\ &= 1 - \exp\left(-\lambda\pi\frac{x^2}{\rho^2}\right),\end{aligned} \tag{3.9}$$

and the pdf

$$f_{r_1}\left(x \mid \frac{r_1}{r_2} \leq \rho\right) = \frac{2\lambda\pi x}{\rho^2} \exp\left(-\lambda\pi\frac{x^2}{\rho^2}\right). \tag{3.10}$$

Now

$$f_{\frac{r_1}{\rho}}\left(x \mid r_1/r_2 \leq \rho\right) = 2\pi\lambda x \exp(-\lambda\pi x^2) = f_{r_1}(x).$$

□

Remark 1. *Theorem 1 shows the SIR gain (in dB) conditioned on the typical user being in $\mathcal{C}_1$ is*

$$G_1 = -10\log_{10}\rho^{\alpha}. \tag{3.11}$$

(3.11) is remarkably simple and directly shows that the top fraction $x = \rho^2$ of users enjoy an SIR gain of $-5\alpha\log_{10} x$ dB relative to the typical user. Here, the "top" users are those with the highest distance ratio of the nearest interferer and the serving BS. Fig. 3.2 shows the SIR gain G_1 as a function of the area fraction of users in $\mathcal{C}_1$. For instance, there are 31.5% of the users that enjoy an average gain of 10 dB over the typical user, and 10% achieve a gain of 20 dB.

Remark 2. *It is interesting to compare this result with the success probability of a*

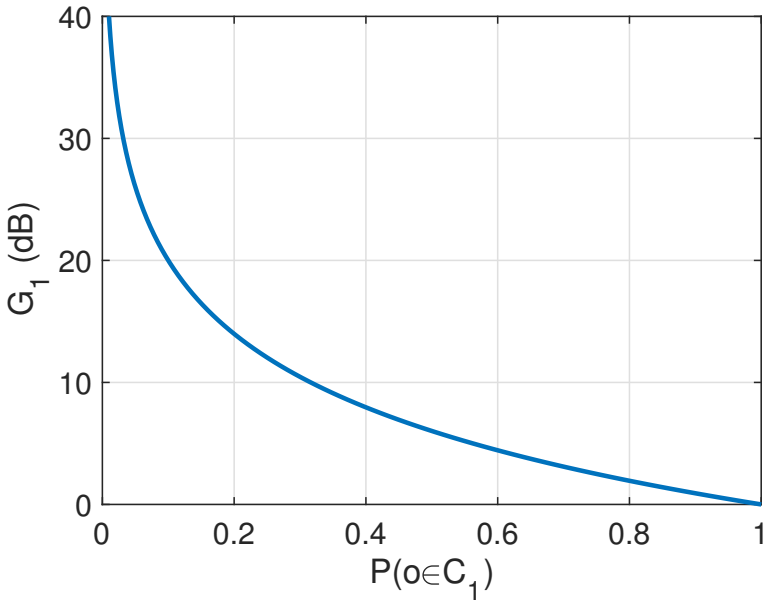

Figure 3.2. The SIR gain (in dB) as a function of the area fraction of $\mathcal{C}_1$, $\alpha = 4$.

BS silencing scheme that mutes all the BSs within r_1/ρ for the typical user, where

$$\begin{aligned}\mathbb{P}(\text{SIR} > \theta) &= \int_0^\infty 2\pi\lambda x \exp\Big(-\pi\lambda x^2 - \int_{\frac{x}{\rho}}^\infty \big(1 - \frac{1}{1+\theta(\frac{x}{t})^\alpha}\big) 2\pi\lambda t \mathrm{d}t\Big)\mathrm{d}x \\ &= \frac{1}{1-\rho^{-2}+\rho^{-2}\ {}_2F_1(1,-\delta;1-\delta;-\rho^\alpha\theta)}.\end{aligned} \tag{3.12}$$

It is easy to show that (3.12) is smaller than (3.7) for any $\theta > 0$ and $\rho \in [0,1]$. This is expected since muting the interfering BSs in r_1/ρ does not affect the ratio of r_1/r_i for $r_i > r_1/\rho$.

Corollary 1. *The gain of the typical user being in $\mathcal{C}_1$ is the same as the gain when all interferers are $1/\rho$ times more distant, i.e.,*

$$r_i' = r_i/\rho, \quad i > 1, \tag{3.13}$$

or, equivalently, the interference power is ρ^α times smaller, i.e., $I' = I\rho^\alpha$.

Proof. Trivial. □

Theorem 1 leads to the evaluation of the conditional success probability, denoted by $P_{\mathrm{s}}(\theta)$, and the SIR meta distribution [24] conditioned on the typical user being in $\mathcal{C}_1$.

Corollary 2. *The b-th moment of the conditional success probability conditioned on the typical user lying in $\mathcal{C}_1$ is*

$$\mathbb{E}[P_{\mathrm{s}}(\theta)^b \mid o \in \mathcal{C}_1] = \frac{1}{{}_2F_1(b, -\delta; 1-\delta; -\rho^\alpha\theta)}, \quad b \in \mathbb{C}. \tag{3.14}$$

and the SIR meta distribution conditioned on the typical user lying in $\mathcal{C}_1$ satisfies

$$\mathbb{P}(P_{\mathrm{s}}(\theta) > x \mid o \in \mathcal{C}_1) = \mathbb{P}(P_{\mathrm{s}}(\rho^\alpha\theta) > x), \quad x \in [0,1]. \tag{3.15}$$

Proof.

$$\begin{aligned}
\mathbb{E}[P_{\mathrm{s}}(\theta)^b \mid o \in \mathcal{C}_1] &= \mathbb{E}\left[\prod_{i=2}^{\infty} \frac{1}{(1+\theta(r_1/r_i)^\alpha)^b} \mid \Phi, o \in \mathcal{C}_1\right] \\
&= \mathbb{E}\left[\prod_{i=2}^{\infty} \frac{1}{(1+\rho^\alpha\theta(r_1/r_i)^\alpha)^b} \mid \Phi\right] \\
&= \frac{1}{{}_2F_1(b, -\delta; 1-\delta; -\rho^\alpha\theta)}.
\end{aligned}$$

Since this holds for any $b \in \mathbb{C}$, it holds for the SIR meta distribution [41]. □

Remark 3. *(3.15) shows that for the same target reliability and percentile, the typical user in $\mathcal{C}_1$ achieves an SIR that is $\rho^{-\alpha}$ times higher than that of the typical user.*

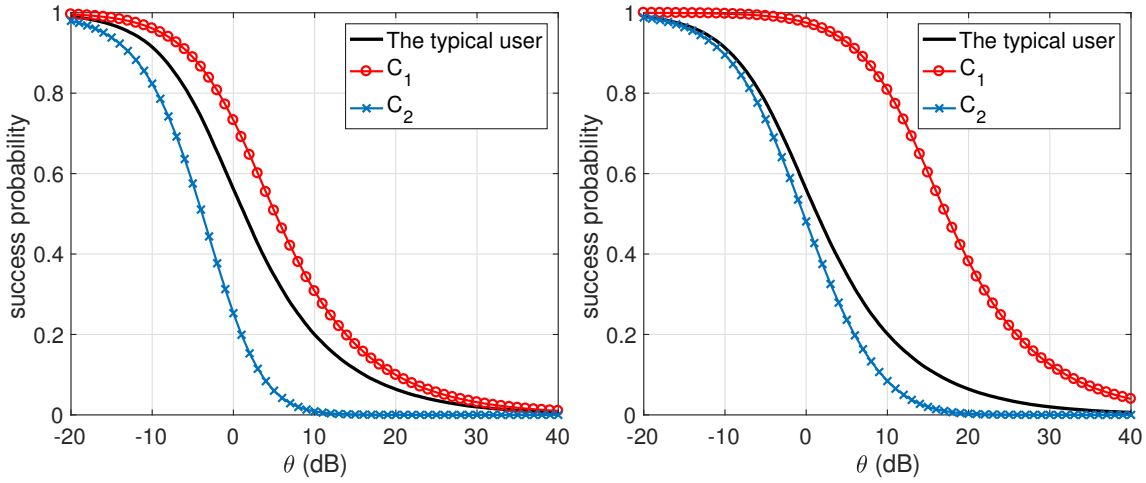

(a) $\gamma = 0.2$. (b) $\gamma = 0.6$.

Figure 3.3. The conditional success probability for the two regions, $\alpha = 4$. The curves for $\mathcal{C}_1$ (red circle) correspond to the curve for the typical user (black) shifted by 3.876 dB and 15.92 dB, respectively.

3.2.2 Cell Boundary Region

Corollary 3. *The success probability conditioned on the typical user being in $\mathcal{C}_2$ is*

$$\mathbb{P}(\mathrm{SIR} > \theta \mid o \in \mathcal{C}_2) = \frac{\bar{F}_{\mathrm{PPP}}(\theta) - \rho^2 \bar{F}_{\mathrm{PPP}}(\theta\rho^\alpha)}{1-\rho^2} \tag{3.16}$$

Proof. Combining (3.2), $\mathbb{P}(o \in \mathcal{C}_2) = 1 - \rho^2$ and the result in Theorem 1, we obtain Corollary 3. □

From (3.16) we notice that the horizontal gain within $\mathcal{C}_2$ is not constant but depends on θ. Fig. 3.3 shows the success probability in the two regions plotted using (3.7) and (3.16). The success probability of the typical user is the weighted average of them.

Taking the limit $\rho \to 1$ of (3.16) we obtain the success probability for the typical

edge user, *i.e.*, the typical user that lies on the edges of the Voronoi cells,

$$\begin{aligned}
&\mathbb{P}(\text{SIR} > \theta \mid x_1(o) = x_2(o)) \\
&= \frac{1}{{}_2F_1(1, -\delta; 1-\delta; -\theta)} - \frac{\theta}{1-\delta} \frac{{}_2F_1(2, 1-\delta; 2-\delta; -\theta)}{{}_2F_1(1, -\delta; 1-\delta; -\theta)^2} \\
&= \frac{1}{(1+\theta)\ {}_2F_1(1, -\delta; 1-\delta; -\theta)^2} \\
&= \frac{\bar{F}_{\text{PPP}}(\theta)^2}{1+\theta}.
\end{aligned}$$

In contrast, for the typical vertex user [27], *i.e.*, the user lying on the vertex of the Voronoi cells,

$$\mathbb{P}(\text{SIR} > \theta \mid x_1(o) = x_2(o) = x_3(o)) = \frac{\bar{F}_{\text{PPP}}(\theta)^2}{(1+\theta)^2}.$$

There is an extra factor $1+\theta$ in the denominator due to the third equidistant BS.

We now calculate the asymptotic SIR gain (the SIR gain as $\theta \to 0$) of the users in $\mathcal{C}_2$. Denote by G_2 the asymptotic SIR gain of the users in $\mathcal{C}_2$ relative to the typical user. Note that $G_2 \leq 1$. We can write the asymptotic form of the success probability of the users in $\mathcal{C}_2$ as [22]

$$\mathbb{P}(\text{SIR} > \theta \mid o \in \mathcal{C}_2) \sim \bar{F}_{\text{PPP}}(\theta/G_2), \quad \theta \to 0, \tag{3.17}$$

where

$$G_2 = \frac{\text{MISR}_{\text{PPP}}}{\text{MISR}_{\mathcal{C}_2}} = \frac{1-\rho^2}{1-\rho^{\alpha+2}}. \tag{3.18}$$

(3.18) follows from the the mean interference-to-signal ratio (MISR) of the typical user $\text{MISR}_{\text{PPP}} = 2/(\alpha-2)$, and the MISR conditioned on the typical user being in

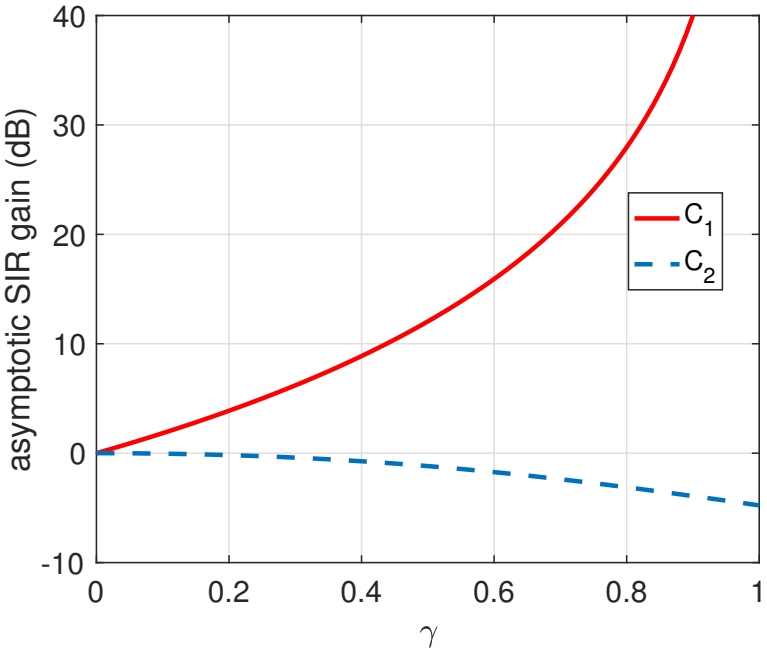

Figure 3.4. The asymptotic SIR gain conditioned on the typical user being in the two regions, $\alpha = 4$.

$\mathcal{C}_2$ as

$$\begin{aligned}
\mathrm{MISR}_{\mathcal{C}_2} &= \mathbb{E}\left[\sum_{i=2}^{\infty}\left(\frac{r_1}{r_i}\right)^{\alpha} \mid o \in \mathcal{C}_2\right] \\
&= \mathbb{E}\left[\left(\frac{r_1}{r_2}\right)^{\alpha} \mid o \in \mathcal{C}_2\right]\left(1 + \mathbb{E}\left[\sum_{i=3}^{\infty}\left(\frac{r_2}{r_i}\right)^{\alpha}\right]\right) \\
&= \frac{2(1-\rho^{\alpha+2})}{(\alpha+2)(1-\rho^2)}\left(1+\frac{4}{\alpha-2}\right) \\
&= \frac{2(1-\rho^{\alpha+2})}{(\alpha-2)(1-\rho^2)}.
\end{aligned}$$

Fig. 3.4 shows the asymptotic SIR gains of the two types of users wrt γ.

Alternatively, we can express the asymptotic success probability using the success probability of the typical edge user and the typical vertex user as baselines. Denote by $G_{2,\mathrm{e}}$, $G_{2,\mathrm{v}}$ the asymptotic gains compared to the typical edge user and the typical vertex user. By combining the typical edge user $\mathrm{MISR}_{\mathrm{e}} = (\alpha+2)/(\alpha-2)$, and the typi-

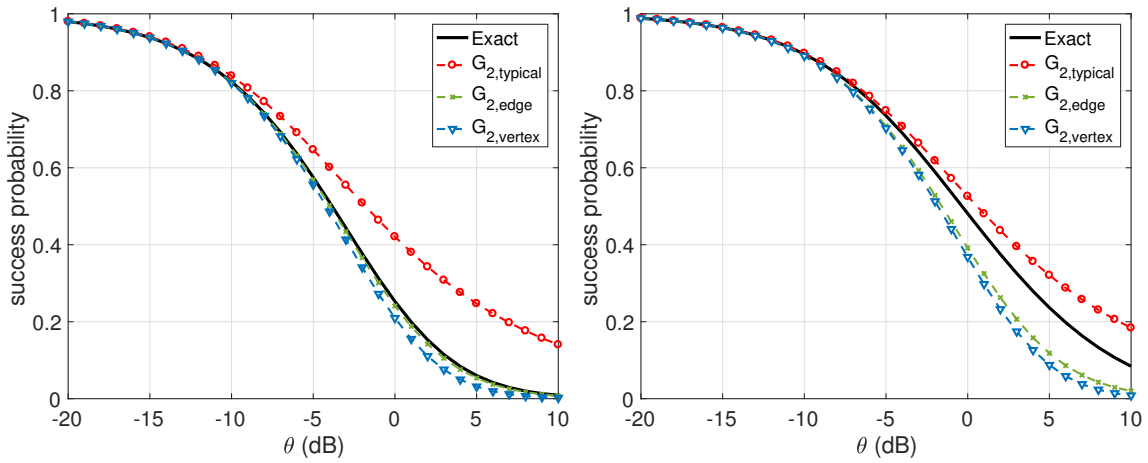

(a) $\gamma = 0.2$. (b) $\gamma = 0.6$.

Figure 3.5. The success probability for the typical user in $\mathcal{C}_2$, $\alpha = 4$. Three approximation curves are plotted, based on the asymptotic SIR gain compared to the typical user, the typical edge user and the typical vertex user.

cal vertex user $\mathrm{MISR}_{\mathrm{v}} = 2\alpha/(\alpha-2)$ [22], we have $G_{2,\mathrm{e}} = (\alpha+2)(1-\rho^2)/(2(1-\rho^{\alpha+2}))$, $G_{2,\mathrm{v}} = \alpha(1-\rho^2)/(1-\rho^{\alpha+2})$ and

$$\begin{aligned}\mathbb{P}(\mathrm{SIR} > \theta \mid o \in \mathcal{C}_2) &\sim \bar{F}_{\mathrm{PPP}}(\theta/G_2) \\ &\sim \frac{\bar{F}_{\mathrm{PPP}}(\theta/G_{2,\mathrm{e}})^2}{1+\theta/G_{2,\mathrm{e}}} \\ &\sim \frac{\bar{F}_{\mathrm{PPP}}(\theta/G_{2,\mathrm{v}})^2}{(1+\theta/G_{2,\mathrm{v}})^2}, \quad \theta \to 0.\end{aligned} \tag{3.19}$$

Fig. 3.5 shows the success probability of the typical user in $\mathcal{C}_2$ and its approximated forms using (3.19). Observe that for large γ, $G_{2,\mathrm{typical}}$ provides a better approximation, while for small γ, $G_{2,\mathrm{edge}}$ provides a better approximation.

3.2.3 Spectral Efficiency

We determine the spectral efficiency in units of nats/s/Hz in an interference-limited scenario assuming rate adaption. The spectral efficiency is defined as

$$R \triangleq \mathbb{E}[\log(1+\mathrm{SIR})] \tag{3.20}$$

and has analytical form $R = \int_0^\infty 1/\big({}_2F_1(1,-\delta;1-\delta;-(e^t-1))\big)\mathrm{d}t$ [18][28].

Letting $R_i \triangleq \mathbb{E}\big[\log(1+\mathrm{SIR}) \mid o \in \mathcal{C}_i\big]$, $i = 1, 2$, we have

$$R = R_1\mathbb{P}(o \in \mathcal{C}_1) + R_2\mathbb{P}(o \in \mathcal{C}_2). \tag{3.21}$$

Corollary 4. *The spectral efficiencies conditioned on the typical user being in* $\mathcal{C}_1$ *and* $\mathcal{C}_2$ *are*

$$R_1 = \int_0^\infty \frac{1}{{}_2F_1(1,-\delta;1-\delta;-\rho^\alpha(e^t-1))}\mathrm{d}t, \tag{3.22}$$

and

$$R_2 = \frac{1}{1-\rho^2}\Big(R - \rho^2 R_1\Big). \tag{3.23}$$

Proof.

$$\begin{aligned} R_1 &= \mathbb{E}\big[\log(1+\mathrm{SIR}) \mid o \in \mathcal{C}_1\big] \\ &= \int_0^\infty \mathbb{P}(\log(1+\mathrm{SIR}) > t \mid o \in \mathcal{C}_1)\mathrm{d}t \\ &= \int_0^\infty \mathbb{P}(\mathrm{SIR} > e^t - 1 \mid o \in \mathcal{C}_1)\mathrm{d}t \\ &= \int_0^\infty \frac{1}{{}_2F_1(1,-\delta;1-\delta;-\rho^\alpha(e^t-1))}\mathrm{d}t. \end{aligned} \tag{3.24}$$

The second part is trivial. □

Fig. 3.6 shows the spectral efficiency conditioned on the typical user being in each region in bits/s/Hz. For instance, when $\alpha = 4$ and $\gamma = 0.4$, $R_1 \approx 4.2$ bits/s/Hz, so

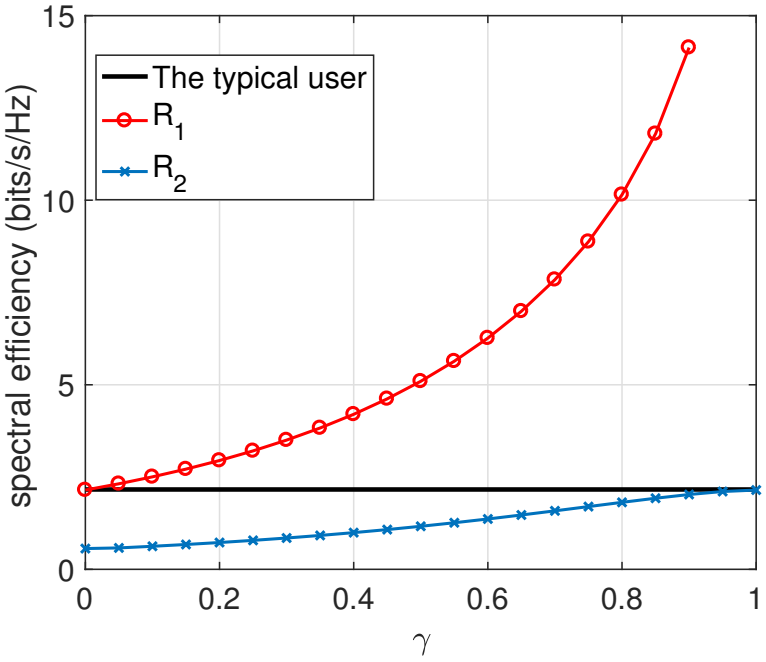

Figure 3.6. The spectral efficiency conditioned on the typical user being in the two regions in comparison with that of the typical user $R = 2.163$ bits/s/Hz (the black line), $\alpha = 4$.

36% of the users achieve almost double of R as a result of good locations. In contrast, the other 64% achieve only $R_2 \approx 0.995$ bits/s/Hz, which is less than half of R as a result of bad locations. R_1 approaches infinity as $\gamma \to 1$ due to the singularity of the power-law path loss function.

3.3 Lattice Networks

In this section, we study the success probability and the asymptotic SIR gain of the cell center region defined in (4.28) in triangular lattice networks. Fig. 3.7 shows the simulated result of the success probability in $\mathcal{C}_1$ with different γ. Fig. 3.8 shows the asymptotic SIR gain G_1 in Poisson networks and triangular lattice networks. The former is plotted using (3.11), and the latter using simulation results evaluated at $p_s(\theta) = 0.95$ with the success probability of the typical user in triangular lattices as

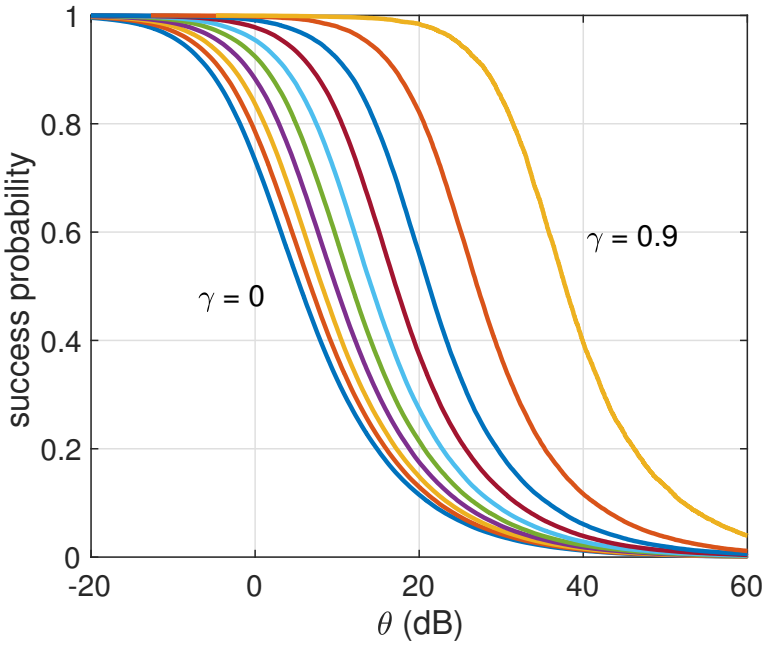

Figure 3.7. The success probability for the typical user in $\mathcal{C}_1$ in triangular lattice networks for $\gamma = 0,\ 0.1,\ ...,\ 0.9$, $\alpha = 4$.

the baseline. The latter is smaller since a user is more likely to have other nearby interfering BSs when fixing the distance ratio between the nearest two BSs.

3.4 Multi-Tier Networks

In this section, we extend our definition of "cell regions" for K-tier networks $\Phi = \bigcup_{i=1}^{K} \Phi_i$, where the i-th tier is modelled using a stationary and ergodic point process $\Phi_i \subset \mathbb{R}^2$, $1 \leq i \leq K$.

Assume that BSs at the i-th tier transmits with power P_i, $1 \leq i \leq K$. For a user u, let $x_i(u)$ be its i-th strongest BS and $v(x_i(u))$ be the index of the tier $x_i(u)$ belongs to, *i.e.*,

$$x_i(u) \in \Phi_{v(x_i(u))}. \tag{3.25}$$

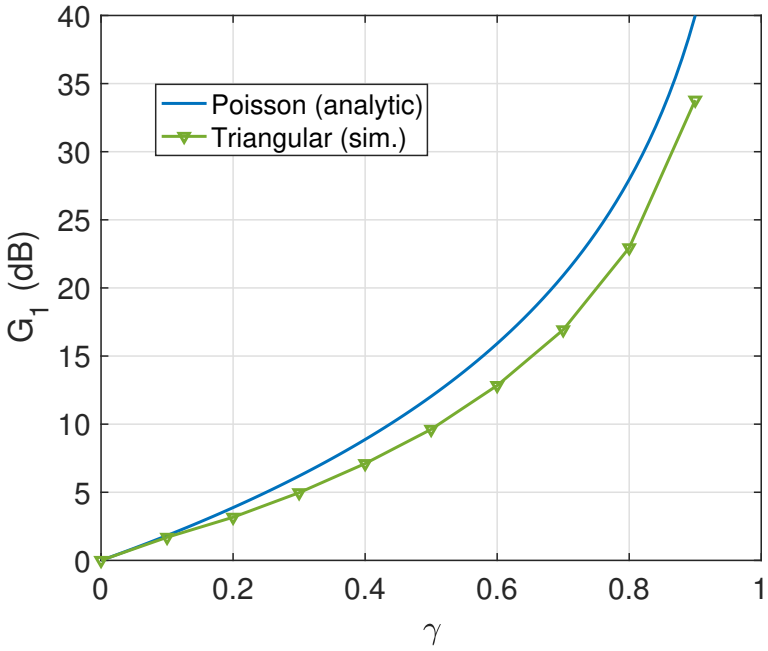

Figure 3.8. The asymptotic SIR gain in the cell center region in Poisson networks and triangular lattice networks, $\alpha = 4$.

We have

$$\frac{\|x_i(u) - u\|}{P_{v(x_i(u))}^{1/\alpha}} \leq \frac{\|x_j(u) - u\|}{P_{v(x_j(u))}^{1/\alpha}}, \quad i \leq j. \tag{3.26}$$

We define

$$\begin{aligned} \mathcal{C}_1 &\triangleq \left\{ u \in \mathbb{R}^2 \colon \frac{\|x_1(u) - u\|}{P_{v(x_1(u))}^{1/\alpha}} \leq \rho \frac{\|x_2(u) - u\|}{P_{v(x_2(u))}^{1/\alpha}} \right\} \\ \mathcal{C}_2 &\triangleq \left\{ u \in \mathbb{R}^2 \colon \rho \frac{\|x_2(u) - u\|}{P_{v(x_2(u))}^{1/\alpha}} < \frac{\|x_1(u) - u\|}{P_{v(x_1(u))}^{1/\alpha}} \right\}, \end{aligned} \tag{3.27}$$

as the "virtual" cell centers and cell boundaries since it is not only distance-based. $K = 1$ retrieves the single-tier case where the regions are defined based on the distances only.

CHAPTER 4

LOCATION-DEPENDENT BASE STATION COOPERATION

The previous analysis shows the disparity in the SIR between different geometric regions. In this chapter, we will exploit the location-dependence of the SIR in BS cooperation schemes where extra resources are allocated to users who need them. Specifically, we focus on joint transmission schemes which turn a set of interfering BSs into cooperating BSs that jointly serve users. Intuitively, turning distant interfering BSs into cooperating BSs would result in inefficient utilization of BS resources (by adding to the cell load), higher computational effort, and extensive backhaul data exchange, since distant BSs have little impact on either the desired signals or the interference. Hence, cooperating BSs should be limited to those close to the user.

From the geometric perspective, users near the Voronoi vertices suffer from strong interference from (at least) two nearby BSs and users near the Voronoi edge suffer from strong interference from (at least) one nearby BS. Extending our definition in Chapter 3, we partition the cells into three regions: the cell center region, the cell edge region, and the cell corner region, based on the relative distances of three nearest BSs. We study the scheme where users in the above regions receive non-coherent joint transmission from one, two, and three nearest BSs, respectively. As such, the scheme primarily helps users with bad locations. The area fraction of each region is tuned by the cooperation level $\gamma \in [0, 1]$.

We analyze the performance of the success probability, the asymptotic SIR gain and the conditional success probability. In particular, the variance of the conditional success probability is studied which serves as a criterion of user fairness in the SIR.

To further evaluate the effectiveness of the scheme under cell load constraints, we study the normalized spectral efficiency, defined as the spectral efficiency normalized by the number of cooperating BSs. We show that the asymptotic SIR gain has a derivative α at $\gamma = 0$ and 0 at $\gamma = 1$, respectively. The user fairness and normalized spectral efficiency both increase first and then decrease with γ. The optimum reliability performance is essentially achieved at $\gamma \approx 0.4$, where the normalized spectral efficiency is decreased by only about 3.4% when $\alpha = 4$.

4.1 BS Cooperation Scheme

4.1.1 Cell Regions and Cooperation Set

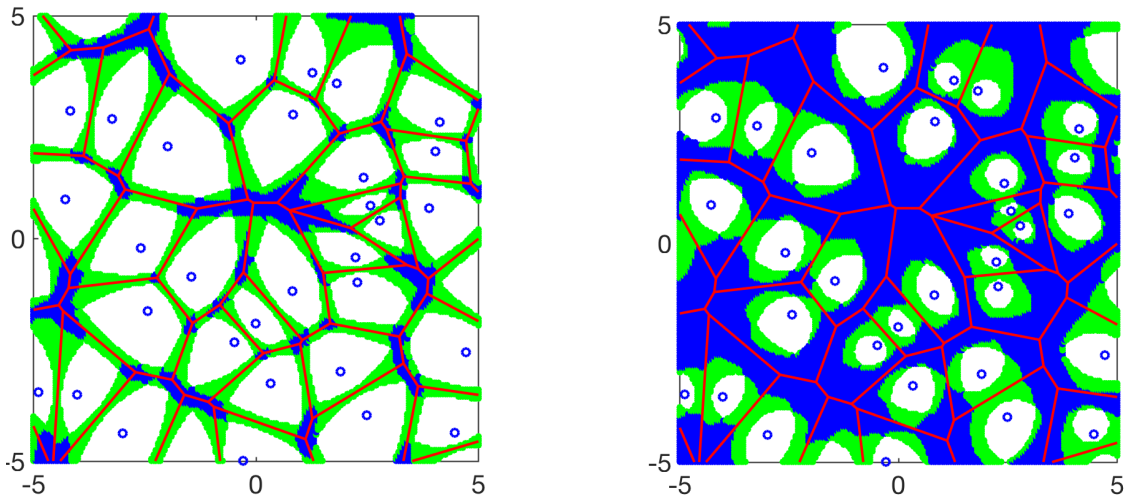

(a) $\gamma = 0.2$. (b) $\gamma = 0.5$.

Figure 4.1. Illustration of the partition when the BSs follow a PPP with intensity $\lambda = 1$ for $\gamma = 0.2$ and $\gamma = 0.5$. The window is $[-5, 5]^2$. Blue circles denote points generated from the PPP. Red lines are the edges of the associated Voronoi cells. Blank, green and blue regions denote the cell center region $\mathcal{C}_1$, the cell edge region $\mathcal{C}_2$, and the cell corner region $\mathcal{C}_3$, respectively.

Let $x_i(u) \in \Phi$ denote the i-th nearest BS in the point process to u. For $\gamma \in [0,1]$ and $\rho = 1-\gamma$ we define

$$\begin{aligned}
\mathcal{C}_1 &\triangleq \{u \in \mathbb{R}^2 \colon \|u - x_1(u)\| \leq \rho \|u - x_2(u)\|\} \\
\mathcal{C}_2 &\triangleq \{u \in \mathbb{R}^2 \colon \rho \|u - x_2(u)\| < \|u - x_1(u)\|, \ \|u - x_1(u)\| \leq \rho \|u - x_3(u)\|\} \\
\mathcal{C}_3 &\triangleq \{u \in \mathbb{R}^2 \colon \|u - x_1(u)\| > \rho \|u - x_3(u)\|\}.
\end{aligned} \tag{4.1}$$

With a slight abuse of notation ($\mathcal{C}_2$ is referred to as "the cell boundary region" in Chapter 3), we refer to $\mathcal{C}_1$, $\mathcal{C}_2$, $\mathcal{C}_3$ as "the cell center region", "the cell edge region", "the cell corner region" respectively. Users within $\mathcal{C}_1$, $\mathcal{C}_2$, $\mathcal{C}_3$ are referred to as "the cell center users", "the cell edge users", and "the cell corner users", respectively. The boundaries of each region $\mathcal{C}_i$ are formed by the union of circular arcs, where for each arc, the two nearest points of Φ are the same and their distance ratio to a point of the arc is ρ.

We define the cooperation set $\mathcal{S}$ to be

$$\mathcal{S} \triangleq \begin{cases} \{x_1(u)\}, & u \in \mathcal{C}_1 \\ \{x_1(u), x_2(u)\}, & u \in \mathcal{C}_2 \\ \{x_1(u), x_2(u), x_3(u)\}, & u \in \mathcal{C}_3. \end{cases} \tag{4.2}$$

In other words, a user in $\mathcal{C}_i$ is jointly served by i BSs since it is relatively close to i BSs.

γ is referred to as the cooperation level since the area fraction of $\mathcal{C}_2 \bigcup \mathcal{C}_3$ increases monotonically with γ. $\gamma = 0$ results in $\mathcal{C}_1 = \mathbb{R}^2$ (no cooperation), and $\gamma = 1$ results in $\mathcal{C}_3 = \mathbb{R}^2 \setminus \Phi$. The special cases $\gamma \in \{0, 1\}$ for the Poisson network have been analyzed in [18, 24] and [25, 34], respectively.

4.1.2 System Model

We consider the non-coherent joint transmission scheme to minimize the constraints on CSI. We focus on the typical user located at the origin o, where the desired signal comes from BSs in the defined cooperation sets and the interference comes from the other BSs. The SIR at the typical user is

$$\mathrm{SIR} = \frac{\left|\sum_{x\in\mathcal{S}} h_x \|x\|^{-\alpha/2}\right|^2}{I}$$

with

$$I \triangleq \sum_{x\in\Phi\setminus\mathcal{S}} |h_x|^2 \|x\|^{-\alpha}.$$

Here, $(h_x)_{x\in\Phi}$ are iid random variables modelling Rayleigh fading, and α denotes the power-law path loss exponent.

4.2 Poisson Networks

We study the performance of the scheme in Poisson networks, where $\Phi \subset \mathbb{R}^2$ is a PPP with intensity λ. Let $r_i = \|x_i(o)\|$ be the distance from the origin to its i-th nearest BS as defined before. The joint distribution of r_1, r_2 and r_3 is [28]

$$f_{r_1,r_2,r_3}(x,y,z) = (2\lambda\pi)^3 xyz \exp\left(-\lambda\pi z^2\right), \quad 0 \le x \le y \le z. \tag{4.3}$$

The area fraction of each region depends on γ and is equal to the probability that the origin falls into each region:

$$\mathbb{P}(o\in\mathcal{C}_1) = (1-\gamma)^2, \quad \mathbb{P}(o\in\mathcal{C}_2) = \gamma(1-\gamma)^2(2-\gamma), \quad \mathbb{P}(o\in\mathcal{C}_3) = \gamma^2(2-\gamma)^2. \tag{4.4}$$

Fig. 4.2 shows the area fraction of the three regions as γ increases from 0 to 1.

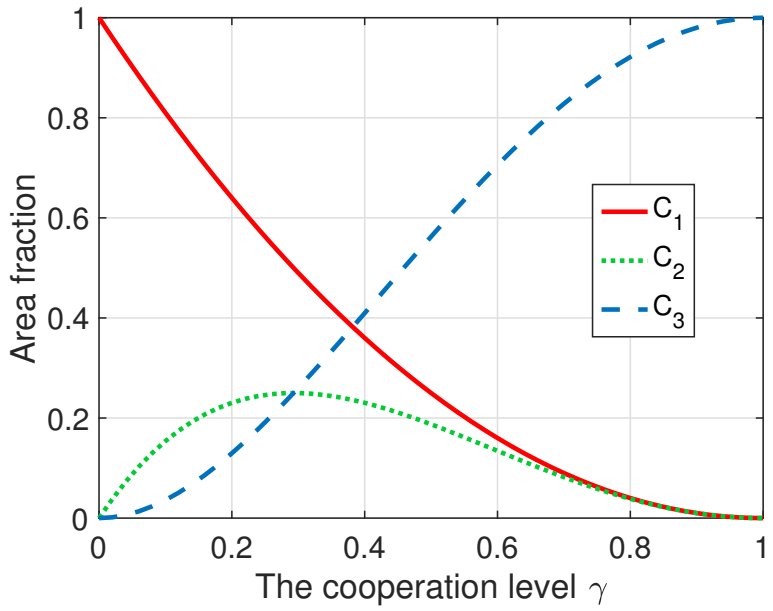

Figure 4.2. The area fraction of the three regions for Poisson networks per (4.4).

Theorem 2. *The asymptotic SIR gain of the proposed BS cooperation scheme in Poisson networks is*

$$G = \frac{2}{(\alpha+2)\mathbb{E}\left[(\frac{r_1}{r_2})^{\alpha}\mathbb{1}_{\mathcal{C}_1}\right] + (\alpha+4)\mathbb{E}\left[\frac{(r_1/r_3)^{\alpha}}{1+(r_1/r_2)^{\alpha}}\mathbb{1}_{\mathcal{C}_2}\right] + 6\mathbb{E}\left[\frac{(r_1/r_3)^{\alpha}}{1+(r_1/r_2)^{\alpha}+(r_1/r_3)^{\alpha}}\mathbb{1}_{\mathcal{C}_3}\right]}. \tag{4.5}$$

For $\alpha = 4$, we have

$$G = \left(\rho^6 + \rho^8\left(\frac{2}{\rho^2} - \frac{\pi}{2} + 2\arctan\rho^2 - 2\right) + 3\int_0^{\infty}\int_x^{\frac{x}{\rho}}\int_{\frac{x}{\rho}}^{\infty} \frac{8xyz^{-3}e^{-z^2}}{x^{-4}+y^{-4}+z^{-4}}\mathrm{d}z\mathrm{d}y\mathrm{d}x\right)^{-1}. \tag{4.6}$$

Proof. The asymptotic SIR gain G can be expressed as

$$G = \frac{\mathrm{MISR}_{\mathrm{PPP}}}{\mathrm{MISR}_{\gamma}}.$$

The MISR of the 2D PPP without cooperation is $\mathrm{MISR}_{\mathrm{PPP}} = 2/(\alpha-2)$ [22], and

$$\mathrm{MISR}_{\gamma} = \mathrm{MISR}_{\mathcal{C}_1} + \mathrm{MISR}_{\mathcal{C}_2} + \mathrm{MISR}_{\mathcal{C}_3},$$

where $\mathrm{MISR}_{\mathcal{C}_i}$ denotes the MISR within $\mathcal{C}_i$. For $\mathcal{C}_1$, we have

$$\mathrm{MISR}_{\mathcal{C}_1} = \sum_{i>1} \mathbb{E}\Big[\Big(\frac{r_1}{r_i}\Big)^{\alpha} \mathbb{1}_{\mathcal{C}_1}\Big] \overset{\text{(a)}}{=} \mathbb{E}\Big[\Big(\frac{r_1}{r_2}\Big)^{\alpha} \mathbb{1}_{\mathcal{C}_1}\Big] \sum_{i>1} \mathbb{E}\Big[\Big(\frac{r_2}{r_i}\Big)^{\alpha}\Big],$$

where step (a) follows from the fact that only the first term in $\mathrm{MISR}_{\mathcal{C}_1}$ is constrained by the cooperation region by Lemma 3. It can be calculated using the joint distribution of r_1 and r_2 as

$$\begin{aligned}\mathbb{E}\Big[\Big(\frac{r_1}{r_2}\Big)^{\alpha} \mathbb{1}_{\mathcal{C}_1}\Big] &= \int_0^{\infty} \int_{\frac{x}{\rho}}^{\infty} f_{r_1,r_2}(x,y) \Big(\frac{r_1}{r_2}\Big)^{\alpha} \mathrm{d}y\mathrm{d}x \\ &= \rho^{\alpha+2}.\end{aligned}$$

The second term can be calculated by considering the relative distance process [3]

$$\sum_{i>1} \mathbb{E}\left[\Big(\frac{r_2}{r_i}\Big)^{\alpha}\right] = 1 + \frac{4}{\alpha-2}.$$

Similarly, we obtain the MISR in $\mathcal{C}_2$ and $\mathcal{C}_3$ as

$$\begin{aligned}\mathrm{MISR}_{\mathcal{C}_2} &= \sum_{i>2} \mathbb{E}\Big[\frac{r_i^{-\alpha}}{r_1^{-\alpha} + r_2^{-\alpha}} \mathbb{1}_{\mathcal{C}_2}\Big] \\ &= \mathbb{E}\Big[\frac{(r_1/r_3)^{\alpha}}{1 + (r_1/r_2)^{\alpha}} \mathbb{1}_{\mathcal{C}_2}\Big] \sum_{i>2} \mathbb{E}\Big[\Big(\frac{r_3}{r_i}\Big)^{\alpha}\Big],\end{aligned} \tag{4.7}$$

where

$$\sum_{i>2} \mathbb{E}\left[\Big(\frac{r_3}{r_i}\Big)^{\alpha}\right] = 1 + \frac{6}{\alpha-2},$$

and

$$\begin{aligned}\mathrm{MISR}_{\mathcal{C}_3} &= \sum_{i>3} \mathbb{E}\Big[\frac{r_i^{-\alpha}}{r_1^{-\alpha}+r_2^{-\alpha}+r_3^{-\alpha}}\mathbb{1}_{\mathcal{C}_3}\Big] \\ &= \mathbb{E}\Big[\frac{(r_1/r_3)^{\alpha}}{1+(r_1/r_2)^{\alpha}+(r_1/r_3)^{\alpha}}\mathbb{1}_{\mathcal{C}_3}\Big]\sum_{i>3}\mathbb{E}\Big[\Big(\frac{r_3}{r_i}\Big)^{\alpha}\Big] \qquad (4.8)\\ &= \int_0^{\infty}\int_x^{\frac{x}{\rho}}\int_{\frac{x}{\rho}}^{\infty}\frac{8xyz^{1-\alpha}e^{-z^2}}{x^{-\alpha}+y^{-\alpha}+z^{-\alpha}}\mathrm{d}z\mathrm{d}y\mathrm{d}x\sum_{i>3}\mathbb{E}\Big[\Big(\frac{r_3}{r_i}\Big)^{\alpha}\Big], \qquad (4.9)\end{aligned}$$

where

$$\sum_{i>3}\mathbb{E}\Big[\Big(\frac{r_3}{r_i}\Big)^{\alpha}\Big] = \frac{6}{\alpha-2}.$$

We obtain the expression for G as in (4.5). □

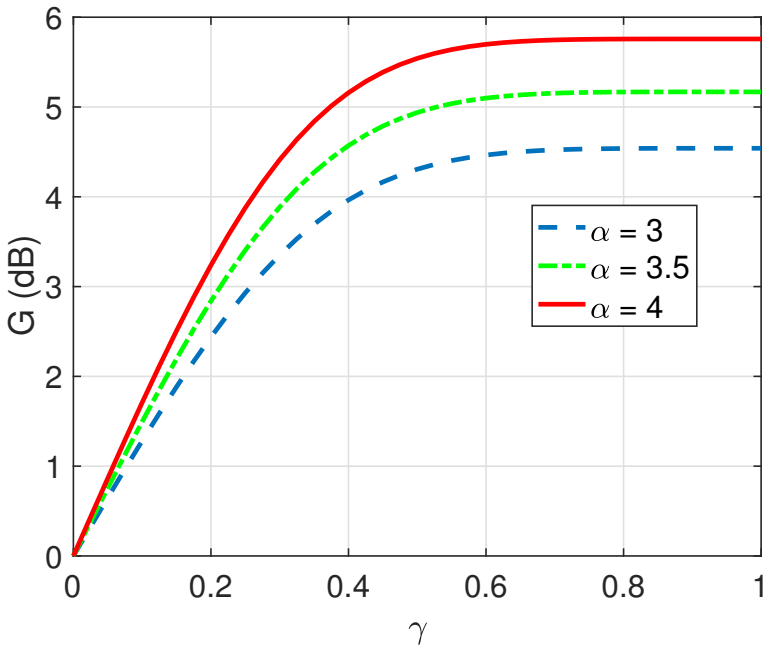

Figure 4.3. The asymptotic gain G (in dB) using (4.5).

We next investigate the derivative of the asymptotic SIR gain.

Corollary 5 (Derivative at $\gamma = 0$ and $\gamma = 1$)**.** *The asymptotic SIR gain G satisfies*

$$\frac{\partial G}{\partial \gamma}\Big|_{\gamma=0} = \alpha, \quad \frac{\partial G}{\partial \gamma}\Big|_{\gamma=1} = 0. \tag{4.10}$$

Proof. For a general α we express G as $G = (G_1 + G_2 + G_3)^{-1}$, where

$$G_1 = (\alpha + 2)\mathbb{E}\Big[\Big(\frac{r_1}{r_2}\Big)^{\alpha} \mathbb{1}_{\mathcal{C}_1}\Big] = \rho^{\alpha+2}, \tag{4.11}$$

$$\begin{aligned} G_2 &= \frac{\alpha+4}{2}\mathbb{E}\Big[\frac{(r_1/r_3)^{\alpha}}{1+(r_1/r_2)^{\alpha}}\mathbb{1}_{\mathcal{C}_2}\Big] \\ &= \frac{\alpha+4}{2}\int_0^{\infty}\int_x^{\frac{x}{\rho}}\int_{\frac{x}{\rho}}^{\infty} 8xyze^{-z^2}\frac{z^{-\alpha}}{x^{-\alpha}+y^{-\alpha}}\mathrm{d}z\mathrm{d}y\mathrm{d}x, \end{aligned} \tag{4.12}$$

$$\begin{aligned} G_3 &= 3\mathbb{E}\Big[\frac{(r_1/r_3)^{\alpha}}{1+(r_1/r_2)^{\alpha}+(r_1/r_3)^{\alpha}}\mathbb{1}_{\mathcal{C}_3}\Big] \\ &= 3\int_0^{\infty}\int_x^{\frac{x}{\rho}}\int_{\frac{x}{\rho}}^{\infty} 8xyze^{-z^2}\frac{z^{-\alpha}}{x^{-\alpha}+y^{-\alpha}+z^{-\alpha}}\mathrm{d}z\mathrm{d}y\mathrm{d}x. \end{aligned} \tag{4.13}$$

Now

$$\frac{\partial G}{\partial \rho} = -G^2\Big(\frac{\partial G_1}{\partial \rho} + \frac{\partial G_2}{\partial \rho} + \frac{\partial G_3}{\partial \rho}\Big),$$

where

$$\frac{\partial G_1}{\partial \rho} = (\alpha+2)\rho^{\alpha+1}, \tag{4.14}$$

$$\frac{\partial G_2}{\partial \rho} = \frac{-4\rho^{1+\alpha}}{1+\rho^{\alpha}} + \frac{\rho^{\alpha-3}(\alpha+4)}{2}\int_0^{\infty}\int_x^{\frac{x}{\rho}} x^3 e^{-\frac{x^2}{\rho^2}}\frac{8y}{1+(x/y)^{\alpha}}\mathrm{d}y\mathrm{d}x, \tag{4.15}$$

and

$$\frac{\partial G_3}{\partial \rho} = -3\rho^{\alpha-3} \int_0^{\infty} \int_x^{\frac{x}{\rho}} x^3 y e^{-\frac{x^2}{\rho^2}} \frac{8}{1+\rho^{\alpha}+(x/y)^{\alpha}} \mathrm{d}y\mathrm{d}x. \tag{4.16}$$

By taking the limit we obtain

$$\frac{\partial G}{\partial \gamma}\Big|_{\gamma=0} = -\lim_{\rho\to 1} \frac{\partial G}{\partial \rho} = \alpha, \tag{4.17}$$

and

$$\frac{\partial G}{\partial \gamma}\Big|_{\gamma=1} = -\lim_{\rho\to 0} \frac{\partial G}{\partial \rho} = 0. \tag{4.18}$$

□

This result shows that the asymptotic gain from $\gamma = 0$ increases with slope α and saturates at $\gamma = 1$. Fig. 4.3 shows the asymptotic SIR gain as γ increases from 0 to 1. When the path loss exponent α grows large, the transmission scenario approaches the point-to-point transmission scenario where the interference is negligible—the interference free scenario. In this case, the network is no longer interference-limited and the effect of noise needs to be considered.

4.2.1 Conditional Success Probability

Lemma 4. *The conditional success probability for the proposed scheme is*

$$P_{\mathrm{s}}(\theta) = \begin{cases} \prod_{i=2}^{\infty} \frac{1}{1+\theta r_i^{-\alpha}/r_1^{-\alpha}}, & o \in \mathcal{C}_1 \\ \prod_{i=3}^{\infty} \frac{1}{1+\theta r_i^{-\alpha}/(r_1^{-\alpha}+r_2^{-\alpha})}, & o \in \mathcal{C}_2 \\ \prod_{i=4}^{\infty} \frac{1}{1+\theta r_i^{-\alpha}/(r_1^{-\alpha}+r_2^{-\alpha}+r_3^{-\alpha})}, & o \in \mathcal{C}_3 \end{cases} \tag{4.19}$$

Proof. For $o \in \mathcal{C}_1$, the typical user is associated with the nearest BS only, hence

$$\begin{aligned} P_{\mathrm{s}}(\theta) &= \mathbb{P}\left(g_1 r_1^{-\alpha} > \theta \sum_{i=2}^{\infty} g_i r_i^{-\alpha} \right) \\ &\overset{\text{(a)}}{=} \mathbb{E}\left[\exp\left(-\theta \sum_{i=2}^{\infty} g_i r_i^{-\alpha} / r_1^{-\alpha} \right) \right] \\ &\overset{\text{(b)}}{=} \mathbb{E}\left[\prod_{i=2}^{\infty} \exp(-\theta g_i r_i^{-\alpha} / r_1^{-\alpha}) \right] \\ &= \prod_{i=2}^{\infty} \frac{1}{1+\theta r_i^{-\alpha} / r_1^{-\alpha}}. \end{aligned} \tag{4.20}$$

Step (a) follows the exponential distribution of the fading power. Step (b) follows from the independence of fading coefficients.

For $o \in \mathcal{C}_2$, the typical user receives the non-coherent joint transmission from two nearest BSs, and thus

$$\begin{aligned} P_{\mathrm{s}}(\theta) &= \mathbb{P}\left(|h_1 r_1^{-\alpha/2} + h_2 r_2^{-\alpha/2}|^2 > \theta \sum_{i=3}^{\infty} g_i r_i^{-\alpha} \right) \\ &\overset{\text{(a)}}{=} \mathbb{E}\left[\prod_{i=3}^{\infty} \exp(-\theta g_i r_i^{-\alpha} / (r_1^{-\alpha} + r_2^{-\alpha})) \right] \\ &= \prod_{i=3}^{\infty} \frac{1}{1+\theta r_i^{-\alpha} / (r_1^{-\alpha} + r_2^{-\alpha})}. \end{aligned} \tag{4.21}$$

Step (a) follows from the fact that $|h_1 r_1^{-\alpha/2} + h_2 r_2^{-\alpha/2}|^2$ is exponentially distributed with mean $r_1^{-\alpha} + r_2^{-\alpha}$.

The proof of $o \in \mathcal{C}_3$ is parallel to that of $o \in \mathcal{C}_2$. □

4.2.2 Moments

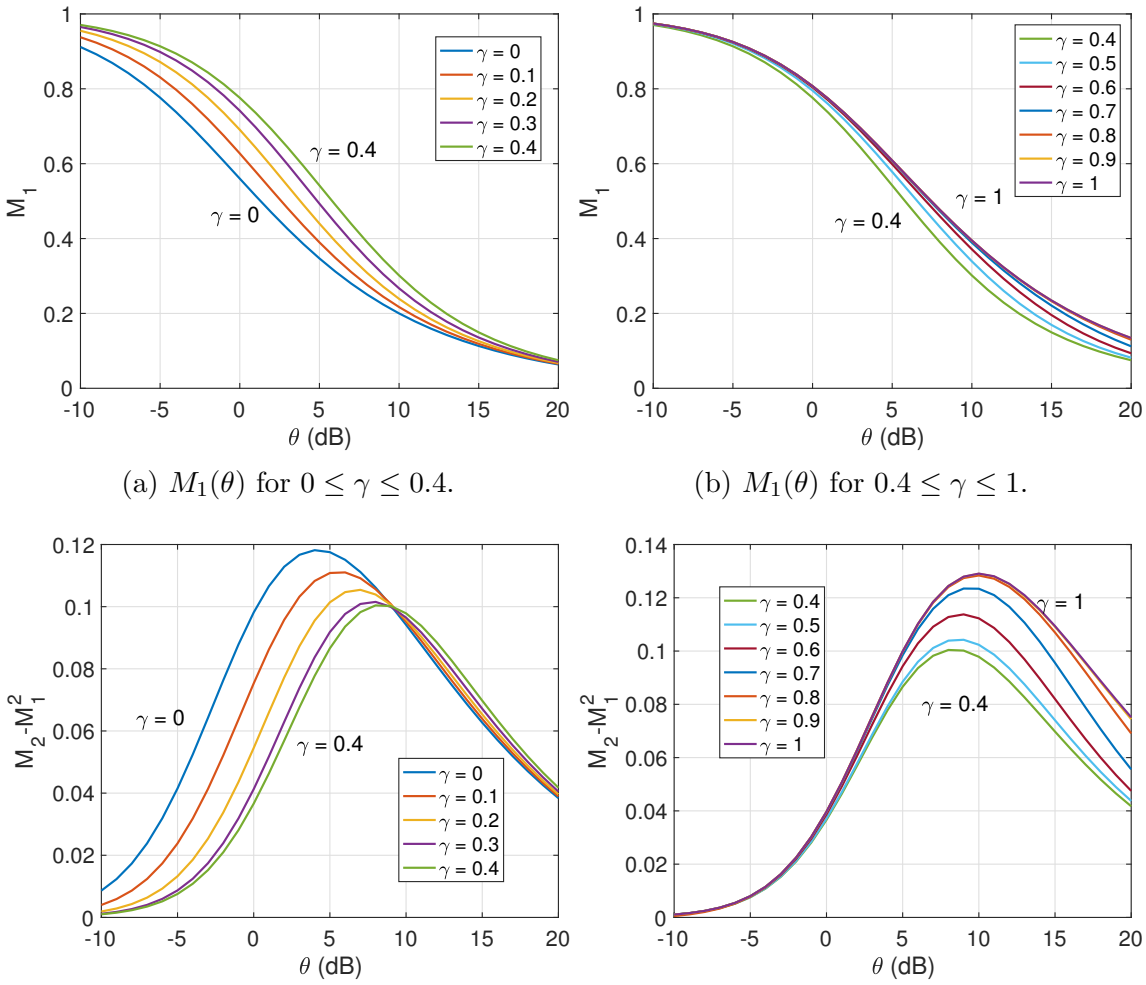

(a) $M_1(\theta)$ for $0 \leq \gamma \leq 0.4$.

(b) $M_1(\theta)$ for $0.4 \leq \gamma \leq 1$.

(c) $M_2(\theta) - M_1(\theta)^2$ for $0 \leq \gamma \leq 0.4$.

(d) $M_2(\theta) - M_1(\theta)^2$ for $0.4 \leq \gamma \leq 1$.

Figure 4.4. The mean $M_1(\theta)$ and variance $M_2(\theta) - M_1(\theta)^2$ of the conditional success probability with cooperation level $\gamma = 0$ to $\gamma = 1$, $\alpha = 4$.

Theorem 3. *The b-th moment of the conditional success probability of the typical user of the proposed scheme in Poisson networks is*

$$\begin{aligned} M_b = & \frac{\rho^2}{{}_2F_1(b,-\delta;1-\delta,-\rho^\alpha\theta)} \\ & + \int_0^\infty \int_x^{\frac{x}{\rho^2}} \int_{\frac{x}{\rho^2}}^\infty \exp\Big(- zF_b\Big(\Big(\frac{z}{x}\Big)^{\frac{1}{\delta}} + \Big(\frac{z}{y}\Big)^{\frac{1}{\delta}}\Big)\Big)\Big(1+\frac{\theta}{\big(\frac{z}{y}\big)^{\frac{1}{\delta}} + \big(\frac{z}{x}\big)^{\frac{1}{\delta}}}\Big)^{-b} \mathrm{d}z\mathrm{d}y\mathrm{d}x \\ & + \int_0^\infty \int_x^{\frac{x}{\rho^2}} \int_y^{\frac{x}{\rho^2}} \exp\Big(- zF_b\Big(1+\Big(\frac{z}{x}\Big)^{\frac{1}{\delta}} + \Big(\frac{z}{y}\Big)^{\frac{1}{\delta}}\Big)\Big)\mathrm{d}z\mathrm{d}y\mathrm{d}x, \quad b\in\mathbb{C}, \end{aligned} \tag{4.22}$$

where $F_b(x) = {}_2F_1(b,-\delta;1-\delta;-\theta/x)$.

Proof.

$$M_b = \mathbb{E}[P_{\mathrm{s}}(\theta)^b] = \sum_{i=1}^3 \mathbb{E}[P_{\mathrm{s}}(\theta)^b \mathbb{1}_{\mathcal{C}_i}]. \tag{4.23}$$

For $\mathcal{C}_1$, we know from Chapter 3 that $\mathbb{E}[P_{\mathrm{s}}(\theta)^b\mathbb{1}_{\mathcal{C}_1}] = \rho^2/{}_2F_1(b,-\delta;1-\delta,-\rho^\alpha\theta)$. For $\mathcal{C}_2$,

$$\mathbb{E}[P_{\mathrm{s}}(\theta)^b\mathbb{1}_{\mathcal{C}_2}] = \mathbb{E}[\prod_{k=3}^\infty \left(\frac{1}{1+\theta r_k^{-\alpha}/(r_1^{-\alpha}+r_2^{-\alpha})}\right)^b \mathbb{1}_{\mathcal{C}_2}] \tag{4.24}$$

$$\begin{aligned} & \overset{\text{(a)}}{=} \int_0^\infty \int_x^{\frac{x}{\rho}} \int_{\frac{x}{\rho}}^\infty \frac{f_{r_1,r_2,r_3}(x,y,z)}{(1+sz^{-\alpha})^b} \exp\Big(- \int_z^\infty \big(1-(1+st^{-\alpha})^{-b}\big)2\pi\lambda t\mathrm{d}t\Big)\mathrm{d}z\mathrm{d}y\mathrm{d}x \\ & \overset{\text{(b)}}{=} \int_0^\infty \int_x^{\frac{x}{\rho^2}} \int_{\frac{x}{\rho^2}}^\infty \frac{\exp(-z)}{(1+sz^{-\alpha/2})^b} \exp\Big(- \int_z^\infty \big(1-(1+st^{-\alpha/2})^{-b}\big)\mathrm{d}t\Big)\mathrm{d}z\mathrm{d}y\mathrm{d}x \\ & \overset{\text{(c)}}{=} \int_0^\infty \int_x^{\frac{x}{\rho^2}} \int_{\frac{x}{\rho^2}}^\infty \exp\Big(- z\ {}_2F_1\Big(b,-\delta,1-\delta,-\frac{s}{z^\alpha}\Big)\Big)(1+sz^{-1})^{-1}\mathrm{d}z\mathrm{d}y\mathrm{d}x. \end{aligned}$$

Step (a) follows from letting $s = \theta/(x^{-\alpha}+y^{-\alpha})$. Step (b) follows from changing

variables $2\pi\lambda x^2$, $2\pi\lambda y^2$, $2\pi\lambda z^2$, $2\pi\lambda t^2$ to x, y, z, t. Step (c) follows from changing variable $t^{\alpha/2}$ to t and $\int_r^\infty (1-1/(1+sx^{-1})^b)x^{\delta-1}\mathrm{d}x = r^\delta(-1+\ {}_2F_1(b,-\delta,1-\delta,-s/r))/\delta$. $\mathbb{E}[P_\mathrm{s}(\theta)^b \mathbb{1}_{\mathcal{C}_3}]$ can be derived by changing the integration region and s. □

We focus on the mean and variance of $P_\mathrm{s}(\theta)$, namely M_1 and $M_2 - M_1^2$. Fig. 4.4 shows the success probability and the variance as a function of θ from $\gamma = 0$ to $\gamma = 1$.

For $0 \leq \gamma \leq 0.4$, the maximal variance is monotonically decreasing when θ is small, and is maximized when the success probability is around $p_s(\theta) = 0.35$. For $\gamma \geq 0.4$, the maximal variance starts monotonically increasing. So the minimal maximal variance is achieved when $\gamma = 0.4$. For $0 \leq \gamma \leq 0.4$, the variance when $\theta > 10$ dB is essentially the same. For $\gamma \geq 0.4$, the variance when $\theta < 0$ dB is essentially the same.

For $\gamma = 1$, the results coincide with the proposed scheme in [25], where all users are served by a fixed number of cooperating BSs. It is shown in [25] that such user-independent BS cooperation increases the unfairness (variance).

Remark 4. *For small θ, the main reason not to succeed is bad fading (fading defines the asymptotic slope of the success probability as $\theta \to 0$). The secondary reason is bad location. Cooperation helps with both, but it makes less of a difference for users in a good location—users near the cell center almost all succeed anyway, even without cooperation. Hence for small θ, M_1 does not change anymore once $\gamma > 0.4$. Similarly, for the variance, all users who need help are receiving it at $\gamma < 0.4$. For larger γ, there is a negligible improvement for most users, hence no further reduction in variance.*

For large θ, the main reason to succeed is good location (proximity to the serving BS defines the asymptotic slope as $\theta \to \infty$). Those users who are quite close to their BS but not extremely close will benefit from cooperation, which means that γ needs to be fairly large (> 0.4) to make a difference in M_1. Conversely, users who get cooperation for $\gamma < 0.4$ are in such bad location that they cannot succeed at high θ.

Similarly, for the variance, for $\gamma < 0.4$ there is no impact since no user switches from not succeeding to succeeding. For $\gamma > 0.4$, the users in almost-great locations start to benefit from cooperation (while those in bad locations still do not), which widens the gap between the two, increasing the variance. This is the regime where "the rich get richer".

4.2.3 Normalized Spectral Efficiency

The normalized spectral efficiency in units of nats/s/Hz/BS is defined as

$$R \triangleq \mathbb{E}\left[\frac{1}{N}\log(1+\mathrm{SIR})\right] \tag{4.25}$$

where $N = |\mathcal{S}|$ is a random variable that depends on the region the typical user falls in. This normalization allows the evaluation of the benefits of cooperation under the constraint of the number of resource blocks a user can occupy.

As shown in the simulation results in Fig. 4.5 (with 100,000 user locations), the ergodic normalized spectral efficiency (in units of bits/s/Hz/BS) increases slightly and then decreases wrt γ. Observe that the same normalized spectral efficiency is guaranteed when $\gamma = 0$ and $\gamma \approx 0.28$. As a result, $\gamma \in [0, 0.28]$ is the range of the cooperation level that improves the typical link quality without lowering the overall throughput. For $\gamma = 0.4$, $R \approx 2.075$ bits/s/Hz/BS, which is about only 3.4% of decrease compared to $R = 2.149$ bits/s/Hz/BS at $\gamma = 0$.

4.3 Lattice Networks

In this section, we apply the scheme to two single-tier lattice networks, namely square lattice and triangular lattice networks. Lattice networks are generally less tractable but they provide upper bounds on the network performance due to the optimistic assumption of BS deployment. Here, we confine our analysis to the asymptotic

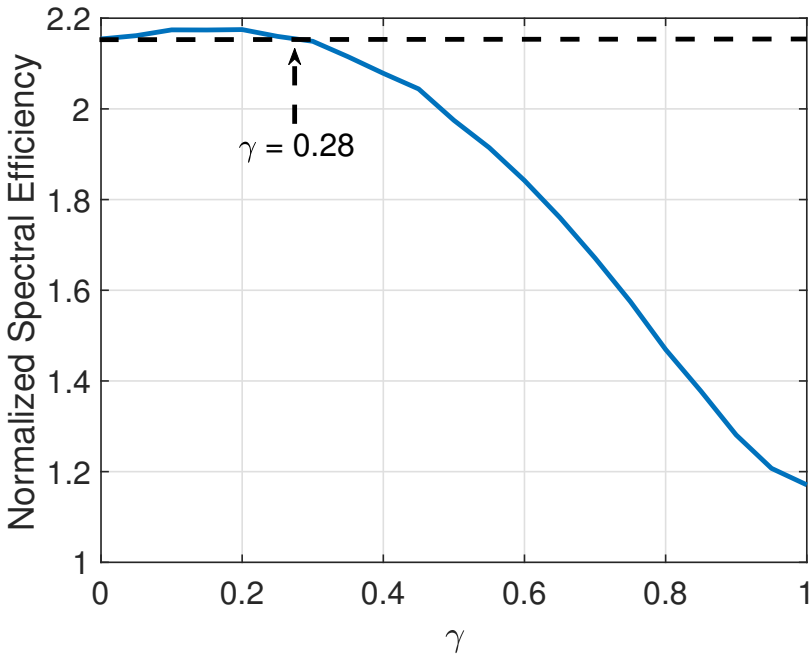

Figure 4.5. The normalized spectral efficiency via simulation, $\alpha = 4$.

SIR gain and make a comparison between Poisson and lattice networks.

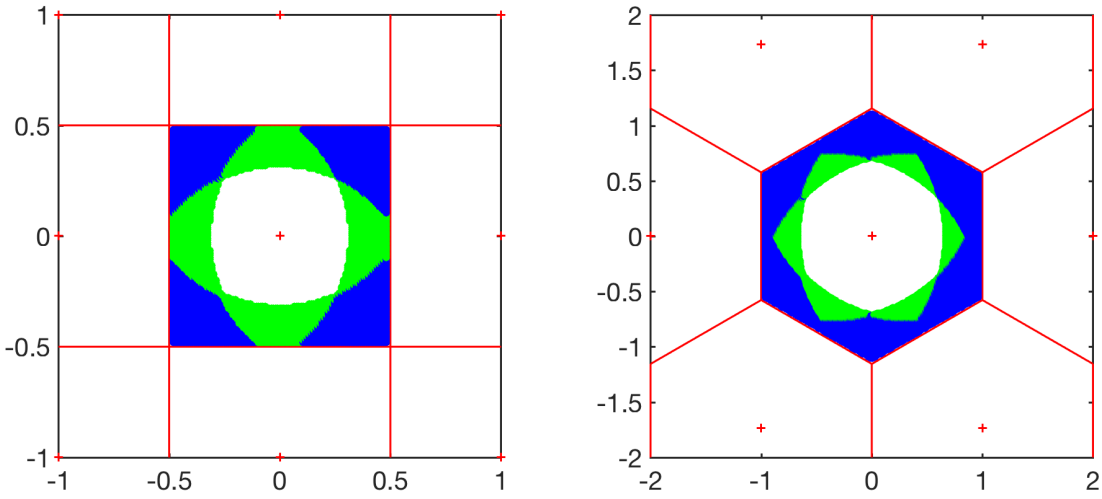

(a) Square lattice

(b) Triangular lattice

Figure 4.6. The cooperation regions in a square lattice and a triangular lattice network when $\gamma = 0.5$. Only one cell is colored since all cells are shifted version of each other. Red crosses and red lines denote BSs and the edges of the associated Voronoi cells in the lattice. Blank, green and blue regions denote $\mathcal{C}_1$, $\mathcal{C}_2$ and $\mathcal{C}_3$ respectively.

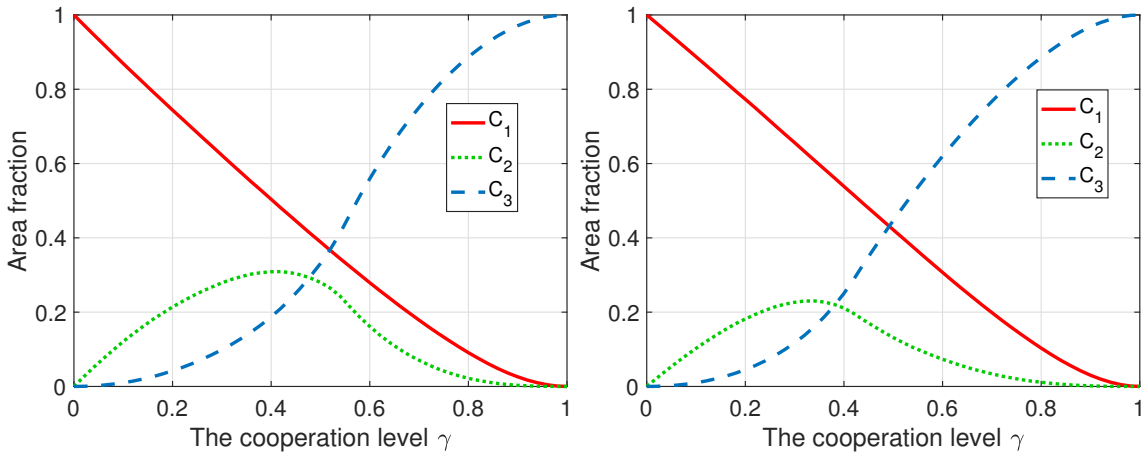

(a) Square lattice (b) Triangular lattice

Figure 4.7. The area fractions of the three regions for square and triangular lattices.

The area fraction of the three regions in lattice networks can be analytically calculated thanks to its rigid structure. The boundaries of each region $\mathcal{C}_i$ are formed by the union of circular arcs, where for each arc, the distance ratio from a point of the arc to its two nearest points is ρ. Note that all the arcs have the same radius and angle depending on γ, as shown in Fig. 4.6. Fig. 4.7 shows the area fraction of each region as γ increases from 0 to 1.

In Fig. 4.8, we compare the asymptotic gain in Poisson networks and lattice networks. The horizontal shift in the lattice cases are approximated using $\tilde{G}_{p_s=0.95}$, *i.e.*, the horizontal SIR shift of the simulated success probability evaluated at $p_s = 0.95$. The simulation is performed with 100,000 user locations. The SIR gap at $\gamma = 0$ is the inherent deployment gain between Poisson and lattice networks (3 dB and 3.4 dB respectively [22]). All three curves increase almost linearly at the beginning and tend to saturate around $\gamma = 0.6$. The comparison reveals the similarity of the SIR gain patterns due to BS cooperation in different network structures.

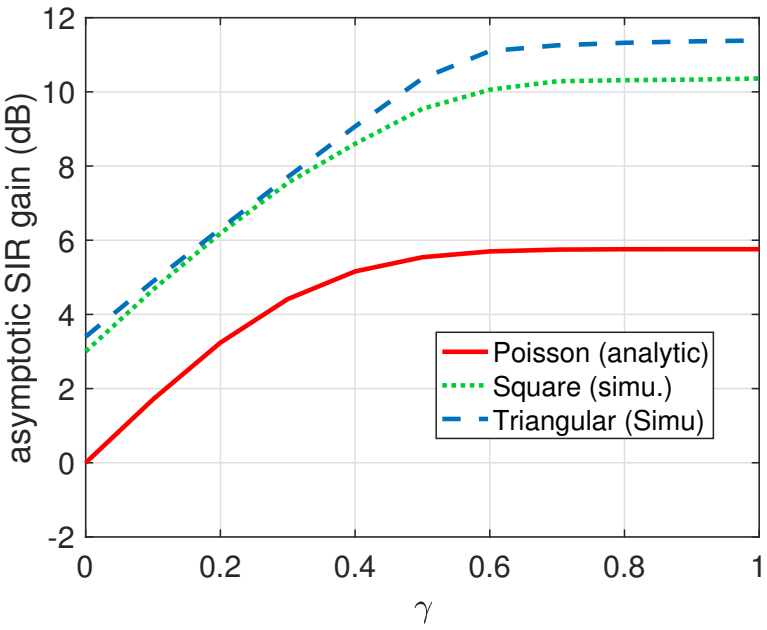

Figure 4.8. The comparison of the asymptotic SIR gain in Poisson networks and lattice networks, $\alpha = 4$.

4.4 Multi-Tier Networks

Multi-tier networks characterize the BS deployment where BSs at different layers have different transmission powers, spatial densities, maximum load, etc. We study a K-tier network $\Phi = \bigcup_{i=1}^{K} \Phi_i$, where the i-th tier is modelled using a stationary and ergodic point process $\Phi_i \subset \mathbb{R}^2$, $1 \leq i \leq K$. We modify our definition of "cell regions" by including the power of each tier. To simplify the analysis, we will limit our partition to three types of users with the maximum number of cooperating BSs being three as before.

4.4.1 Cell Regions and Cooperation Set

Assume BSs at the i-th tier transmits with power P_i, $1 \leq i \leq K$. For a user at location u, let $x_i(u)$ be its i-th strongest BS and $v(x_i(u))$ be the index of the tier $x_i(u)$ belongs to, *i.e.*,

$$x_i(u) \in \Phi_{v(x_i(u))}. \tag{4.26}$$

We have

$$\frac{\|x_i(u)-u\|}{P_{v(x_i(u))}^{1/\alpha}} \leq \frac{\|x_j(u)-u\|}{P_{v(x_j(u))}^{1/\alpha}}, \quad i \leq j. \tag{4.27}$$

Letting $\rho = 1-\gamma$ we define

$$\begin{aligned}
\mathcal{C}_1 &\triangleq \left\{u \in \mathbb{R}^2 \colon \frac{\|x_1(u)-u\|}{P_{v(x_1(u))}^{1/\alpha}} \leq \rho \frac{\|x_2(u)-u\|}{P_{v(x_2(u))}^{1/\alpha}}\right\} \\
\mathcal{C}_2 &\triangleq \left\{u \in \mathbb{R}^2 \colon \rho\frac{\|x_2(u)-u\|}{P_{v(x_2(u))}^{1/\alpha}} < \frac{\|x_1(u)-u\|}{P_{v(x_1(u))}^{1/\alpha}}, \ \frac{\|x_1(u)-u\|}{P_{v(x_1(u))}^{1/\alpha}} \leq \rho\frac{\|x_3(u)-u\|}{P_{v(x_3(u))}^{1/\alpha}}\right\} \\
\mathcal{C}_3 &\triangleq \left\{u \in \mathbb{R}^2 \colon \frac{\|x_1(u)-u\|}{P_{v(x_1(u))}^{1/\alpha}} > \rho \frac{\|x_3(u)-u\|}{P_{v(x_3(u))}^{1/\alpha}}\right\}.
\end{aligned} \tag{4.28}$$

For a cooperation level γ we partition the plane into three regions based on the relative average received signal strength to the three strongest BSs. The order is determined jointly by the power and distance of the BSs. Intuitively, each user has a list of potential serving BSs in the network that have descending average channel quality. A user within $\mathcal{C}_1$ receives a much stronger signal from its serving BS than from all the interfering ones; a user within $\mathcal{C}_2$ receives signals of similar strength from two strongest BSs and much weaker signals from the interfering ones; $\mathcal{C}_3$ is defined analogously. The cooperation scheme is that a user receiving similar signal strength from i BSs is jointly served by i BSs. γ defines "similarity" in a rigorous way.

$K = 1$ is the single-tier case where the regions are defined based on the distances only.

4.4.2 Homogeneous Independent Poisson Networks

The homogeneous independent Poisson (HIP) model [22, Def. 2] is a K-tier network, where the i-th tier BSs are modeled as a homogeneous PPP $\Phi_i \subset \mathbb{R}^2$ with intensity λ_i and transmit with power P_i. The independence between Φ_is is assumed.

We focus on the typical user at the origin o. Let $\Xi = \bigcup_{i=1}^{K} \{\|x\|^{\alpha} / P_{v(x)}\}$, we obtain the distance process (DP)—a non-homogeneous PPP on $\mathbb{R}^+$. Its intensity function is

$$\lambda(t) = \sum_{i=1}^{K} \lambda_i \pi \delta P_i t^{\delta - 1}, \quad t \in \mathbb{R}^+, \tag{4.29}$$

where $\delta = 2/\alpha$. Arranging the elements in Ξ in ascending order, we have $\xi_i = \|x_i(o)\|^{\alpha} / P_{v(x_i(o))}$ where $\xi_1 < \xi_2 < ....$ Note that ξ_i^{-1} is the average received signal power from the i-th strongest BS.

The joint distribution of $\xi_1 < \xi_2 < \xi_3$ is given by [34] as

$$f_{\xi_1,\xi_2,\xi_3}(x, y, z) = (\lambda_{\text{eq}} \pi \delta)^3 \exp\left(-\lambda_{\text{eq}} \pi z^{\delta}\right) (xyz)^{\delta - 1}, \quad 0 \le x \le y \le z, \tag{4.30}$$

where $\lambda_{\text{eq}} = \sum_{i=1}^{K} \lambda_i P_i^{\delta}$.

The success probability is independent of the number of network tiers K and the power level P_i in each tier [34], so is the meta distribution [42]. The evaluation of the metrics of interest is omitted, since this generalization to multi-tier networks is but a redefinition of the three regions.

CHAPTER 5

CONCLUSIONS AND FUTURE WORK

In this thesis, we develop a location-dependent SIR analysis based on cell regions in cellular networks. The definition of "the cell edge region" ("the cell corner region") is based on the relative distances between the nearest two (three) BSs. We show that in Poisson networks, the top fraction x of users enjoy an SIR gain of $-5\alpha \log_{10} x$ dB relative to the typical user. To mitigate the interference, we propose a location-dependent BS cooperation scheme that primarily helps users in bad locations. The cooperation level γ is introduced to tune the area fraction of cell regions, which gives the room for optimization. By defining the three regions where users get served by one, two, and three nearest BSs, the reliability performance can be improved without sacrificing spectral efficiency. In fact, there is a regime of γ where both can be improved. The optimum reliability performance is achieved at $\gamma \approx 0.4$, where the normalized spectral efficiency is decreased only about 3.4%. BS cooperation with γ beyond the optimum level will essentially not improve the reliability performance but increase the cell load. Therefore, BS cooperation should focus on users in disadvantaged locations.

This work permits many potential extensions. For instance, in this thesis we consider a special case of heterogeneous networks. It can be extended to BS models where the repulsion within each tier and dependence between tiers are considered. The proposed definition of cell regions can be applied in the scenario of handover to avoid frequent handovers in dense networks—mobile users in the cell corner region may not need switch even if the serving BS is not the nearest (strongest) one.

This work can be combined with user distributions to facilitate the analysis of intra-cell/inter-cell multi-user scheduling and interference management in the uplink. The proposed framework can also be used in interference coordination for non-orthogonal multiple access (NOMA) transmission techniques. Lastly, it would be interesting to explore the similarities and differences between the notion of top users in the cell center region and that of the SIR meta distribution.

BIBLIOGRAPHY

1. J. Xu, J. Zhang, and J. G. Andrews, "On the accuracy of the Wyner model in cellular networks," *IEEE Transactions on Wireless Communications*, vol. 10, pp. 3098–3109, Sep 2011.

2. A. Guo and M. Haenggi, "Spatial stochastic models and metrics for the structure of base stations in cellular networks," *IEEE Transactions on Wireless Communications*, vol. 12, pp. 5800–5812, Nov 2013.

3. R. K. Ganti and M. Haenggi, "Asymptotics and approximation of the SIR distribution in general cellular networks," *IEEE Transactions on Wireless Communications*, vol. 15, pp. 2130–2143, Mar 2016.

4. S. S. Kalamkar and M. Haenggi, "Simple approximations of the SIR meta distribution in general cellular networks," *IEEE Transactions on Communications*, 2019. Accepted.

5. C. E. Shannon, "A mathematical theory of communication," *The Bell System Technical Journal*, vol. 27, pp. 379–423, Jul 1948.

6. D. Gesbert, S. Hanly, H. Huang, S. S. Shitz, O. Simeone, and W. Yu, "Multi-cell MIMO cooperative networks: A new look at interference," *IEEE Journal on Selected Areas in Communications*, vol. 28, pp. 1380–1408, Dec 2010.

7. R. Irmer, H. Droste, P. Marsch, M. Grieger, G. Fettweis, S. Brueck, H.-P. Mayer, L. Thiele, and V. Jungnickel, "Coordinated multipoint: Concepts, performance, and field trial results," *IEEE Communications Magazine*, vol. 49, pp. 102–111, Feb 2011.

8. S. N. Chiu, D. Stoyan, W. S. Kendall, and J. Mecke, *Stochastic geometry and its applications*. John Wiley & Sons, 2013.

9. J. Moller, *Lectures on random Voronoi tessellations*, vol. 87. Springer Science & Business Media, 2012.

10. D. J. Daley and D. Vere-Jones, *An introduction to the theory of point processes: volume II: general theory and structure*. Springer Science & Business Media, 2007.

11. M. Haenggi, *Stochastic geometry for wireless networks*. Cambridge University Press, 2012.

12. F. Baccelli and B. Baszczyszyn, "Stochastic geometry and wireless networks: Volume I theory," *Foundations and Trends in Networking*, vol. 3, no. 34, pp. 249–449, 2010.

13. F. Baccelli and B. Baszczyszyn, "Stochastic geometry and wireless networks: Volume II applications," *Foundations and Trends in Networking*, vol. 4, no. 1–2, pp. 1–312, 2010.

14. B. Blaszczyszyn, M. Haenggi, P. Keeler, and S. Mukherjee, *Stochastic Geometry Analysis of Cellular Networks*. Cambridge University Press, 2018.

15. F. Baccelli, M. Klein, M. Lebourges, and S. Zuyev, "Stochastic geometry and architecture of communication networks," *Telecommunication Systems*, vol. 7, pp. 209–227, Jun 1997.

16. M. Haenggi, J. G. Andrews, F. Baccelli, O. Dousse, and M. Franceschetti, "Stochastic geometry and random graphs for the analysis and design of wireless networks," *IEEE Journal on Selected Areas in Communications*, vol. 27, pp. 1029–1046, Sep 2009.

17. H. ElSawy, E. Hossain, and M. Haenggi, "Stochastic geometry for modeling, analysis, and design of multi-tier and cognitive cellular wireless networks: A survey," *IEEE Communications Surveys Tutorials*, vol. 15, pp. 996–1019, Third 2013.

18. J. G. Andrews, F. Baccelli, and R. K. Ganti, "A tractable approach to coverage and rate in cellular networks," *IEEE Transactions on Communications*, vol. 59, pp. 3122–3134, Nov 2011.

19. N. Ross and D. Schuhmacher, "Wireless network signals with moderately correlated shadowing still appear Poisson," *IEEE Transactions on Information Theory*, vol. 63, pp. 1177–1198, Feb 2017.

20. N. Deng, W. Zhou, and M. Haenggi, "The Ginibre point process as a model for wireless networks with repulsion," *IEEE Transactions on Wireless Communications*, vol. 14, pp. 107–121, Jan 2015.

21. D. Lopez-Perez and M. Ding, "A brief history on the theoretical analysis of dense small cell wireless networks," *arXiv e-prints*, p. arXiv:1812.02269, Dec 2018.

22. M. Haenggi, "The mean interference-to-signal ratio and its key role in cellular and amorphous networks," *IEEE Wireless Communications Letters*, vol. 3, pp. 597–600, Dec 2014.

23. A. AlAmmouri, J. G. Andrews, and F. Baccelli, "SINR and throughput of dense cellular networks with stretched exponential path loss," *IEEE Transactions on Wireless Communications*, vol. 17, pp. 1147–1160, Feb 2018.

24. M. Haenggi, "The meta distribution of the SIR in Poisson bipolar and cellular networks," *IEEE Transactions on Wireless Communications*, vol. 15, pp. 2577–2589, Apr 2016.

25. Q. Cui, X. Yu, Y. Wang, and M. Haenggi, "The SIR meta distribution in Poisson cellular networks with base station cooperation," *IEEE Transactions on Communications*, vol. 66, pp. 1234–1249, Mar 2018.

26. S. S. Kalamkar and M. Haenggi, "The spatial outage capacity of wireless networks," *IEEE Transactions on Wireless Communications*, vol. 17, pp. 3709–3722, Jun 2018.

27. S. Y. Jung, H. Lee, and S. Kim, "Worst-case user analysis in Poisson Voronoi cells," *IEEE Communications Letters*, vol. 17, pp. 1580–1583, Aug 2013.

28. X. Zhang and M. Haenggi, "A stochastic geometry analysis of inter-cell interference coordination and intra-cell diversity," *IEEE Transactions on Wireless Communications*, vol. 13, pp. 6655–6669, Dec 2014.

29. K. Feng and M. Haenggi, "A tunable base station cooperation scheme for Poisson cellular networks," in *2018 52nd Annual Conference on Information Sciences and Systems (CISS)*, pp. 1–6, Mar 2018.

30. R. Tanbourgi, S. Singh, J. G. Andrews, and F. K. Jondral, "A tractable model for noncoherent joint-transmission base station cooperation," *IEEE Transactions on Wireless Communications*, vol. 13, pp. 4959–4973, Sep 2014.

31. F. Baccelli and A. Giovanidis, "A stochastic geometry framework for analyzing pairwise-cooperative cellular networks," *IEEE Transactions on Wireless Communications*, vol. 14, pp. 794–808, Feb 2015.

32. A. Lozano, R. W. Heath, and J. G. Andrews, "Fundamental limits of cooperation," *IEEE Transactions on Information Theory*, vol. 59, pp. 5213–5226, Sep 2013.

33. J. Yoon and G. Hwang, "Distance-based inter-cell interference coordination in small cell networks: Stochastic geometry modeling and analysis," *IEEE Transactions on Wireless Communications*, vol. 17, pp. 4089–4103, Jun 2018.

34. G. Nigam, P. Minero, and M. Haenggi, "Coordinated multipoint joint transmission in heterogeneous networks," *IEEE Transactions on Communications*, vol. 62, pp. 4134–4146, Nov 2014.

35. H. S. Dhillon, R. K. Ganti, F. Baccelli, and J. G. Andrews, "Modeling and analysis of K-tier downlink heterogeneous cellular networks," *IEEE Journal on Selected Areas in Communications*, vol. 30, pp. 550–560, Apr 2012.

36. A. H. Sakr and E. Hossain, "Location-aware cross-tier coordinated multipoint transmission in two-tier cellular networks," *IEEE Transactions on Wireless Communications*, vol. 13, pp. 6311–6325, Nov 2014.

37. Q. Ye, B. Rong, Y. Chen, M. Al-Shalash, C. Caramanis, and J. G. Andrews, "User association for load balancing in heterogeneous cellular networks," *IEEE Transactions on Wireless Communications*, vol. 12, pp. 2706–2716, Jun 2013.

38. L. Liu, S. Zhang, and R. Zhang, "CoMP in the sky: UAV placement and movement optimization for multi-user communications," *arXiv e-prints*, p. arXiv:1802.10371, Feb 2018.

39. Y. Sun, Z. Ding, and X. Dai, "A user-centric cooperative scheme for UAV assisted wireless networks in malfunction areas," *arXiv e-prints*, p. arXiv:1902.01940, Jan 2019.

40. K. Feng and M. Haenggi, "On the location-dependent SIR gain in cellular networks," *IEEE Wireless Communications Letters*, pp. 1–1, Jan 2019 (Early Access).

41. M. Haenggi, "Efficient calculation of meta distributions and the performance of user percentiles," *IEEE Wireless Communications Letters*, vol. 7, pp. 982–985, Dec 2018.

42. Y. Wang, M. Haenggi, and Z. Tan, "SIR meta distribution of K-tier downlink heterogeneous cellular networks with cell range expansion," *IEEE Transactions on Communications*, pp. 1–1, 2018. Accepted.